section because of their more benign character. More favorable outcomes can be achieved with aggressive surgical intervention, ranging from partial to gross total removal.

For malignant gliomas, on the other hand, surgical intervention is generally not indicated, because their prognosis remains so poor and is not improved by surgery.[5,11,12,19,20,26] Most patients with malignant brainstem gliomas die within 1 year and rarely survive more than 18 months, even when treated.[11,12,14,18,30,34,36,37,39,46,47] Several cases of gross total resection of malignant gliomas of the brainstem, outside the medulla oblongata, have been reported with poor outcome.[1,3–5,12] Epstein et al.,[3–5] reported that of paediatric cases undergoing radical resection of intrinsic malignant gliomas of the pons or cervicomedullary junction, the majority of patients died within 12–18 months without significantly benefiting from surgery. Furthermore, despite recent advances in neuroimaging, surgical equipment, microsurgical technology and anatomical knowledge, radical surgical excision of intra-axial tumors of the medulla oblongata remains rare because the medulla oblongata performs such important vital functions. Extensive dissection in this region may result in significant morbidity and mortality. Some reports have dealt with a few patients with benign tumors, rarely malignant gliomas, of the medulla oblongata, undergoing gross total removal.[12,26,27] Abbott et al.,[27] reported on 6 pediatric patients with intrinsic gliomas of the medulla oblongata, who underwent radical excision. One of them had a glioblastoma multiforme and died from tumor progression 3 months postoperatively. Three continued to suffer from permanent postoperative swallowing dysfunction. Of our two patients, who underwent gross total removal of intrinsic and exophytic malignant gliomas in the medulla oblongata, although one patient (case 2) experienced neurological deterioration, the other (patient 1) showed symptomatic improvement. The patient with an anaplastic astrocytoma survived 3 years and 9 months, and the patient with a glioblastoma multiforme 2 years and 3 months. This is longer than the anticipated survival of patients with malignant brainstem gliomas.

### Anatomical and symptomatological considerations[48]

The medulla oblongata is approximately 2.5–3 cm long from the pontomedullary junction to the roots of C1 (Fig. 6, left). The pyramidal tract is found in the most anterior part of the medulla oblongata, while the medial longitudinal fascicle (MLF) runs under the posterior surface just lateral to the median sulcus. The dorsal aspect of the upper half of the medulla oblongata consists mainly of the lower third of the rhomboid fossa (fourth ventricle floor). Internal structures at this level include the dorsal vagal, hypoglossal, ambiguous and inferior olivary nuclei, and the nucleus of the solitary tract. The medial lemniscus originates from under the posterior surface near the caudal edge of the fourth ventricle floor, and runs upward deeply and anteriorally within the medulla oblongata coursing posterior to the pyramidal tracts. The dorsal aspect of the lower half of the medulla oblongata consists of the posterior funiculi containing the nuclei gracilis medially and the nuclei cuneatus laterally. These continue to the medial lemnisci.

The autonomic centers participating in swallowing, respiratory and cardiovascular functions are located in the reticular formation in the upper half of the medulla oblongata (ventricular part), especially in the medial area, but not in the lower half (funicular part). Various other nuclei and structures in the upper half of the medulla oblongata also participate in these functions. The center of swallowing is located near the motor nuclei of cranial nerves. The ambiguous and hypoglossal nuclei, and the nucleus of the solitary tract also participate in swallowing. The respiratory center is located dorsally to the inferior olivary nucleus. The vagal dorsal nucleus and the nucleus of the solitary tact are components of reflex arcs controlling respiratory as well as cardiovascular functions. The center for cardiovascular control is located in the vicinity of the ambiguous nucleus. Complete unilateral interruption of the vagus nerve may cause some dysphagia as well as occasional tachycardia and arrhythmia. Complete bilateral paralysis of the vagus nerve invariably causes death. A feedback loop participating in cerebellar function extends from the red nucleus of the midbrain to the inferior olive via the central tegmental tract, and from there to the contralateral dentate nucleus of the cerebellum via the olivocerebellar tract, running through the inferior cerebellar peduncle, and back to the red nucleus (the triangle of Guillain–Mollaret). Damage to this cerebellar feedback circuit at the level of the medulla oblongata may cause cerebellar dysfunction such as gait disturbance. Injury to the MLF running in the medulla oblongata may lead to nystagmus. Structures participating in position sense are the fasciculi gracilis and cuneatus as well as the homonymous nuclei and the medial lemnisci. The sensory impulses coming from the lower extremity are transferred to the nucleus gracilis through the fasciculus gracilis, while those from the upper extremity are transferred to the nucleus cuneatus through the fasciculus cuneatus.

The 3-dimensional topography of the relevant anatomical structures of the medulla oblongata is shown in Fig. 6 (left).

### Surgical considerations

It has been thought that direct surgery on the medulla oblongata had the inherent risk of causing serious complications leading to a fatal outcome. From an anatomical point of view, the important vital structures are situated mainly in the upper half of the medulla oblongata, particularly on the medial side. Hence, if a surgeon approaches posteriorally to the medial part of the upper medulla oblongata, it can endanger critical vital centers, including the medial lemniscus and the nucleus gracilis. However, approaching via the lateral part of the upper medulla may have a lower risk of damaging the critical structures in comparison to a medial approach. A lateral approach is likely to jeopardize the sensory tracts, especially the fasciculus or nucleus cuneatus. The approach to the posterior midportion of the upper half of the medulla oblongata may have the highest risk of causing significant morbidity and mortality. If a tumor extends or is located anteromedially, there is a further risk of damaging the pyramidal tract.

In the cases presented here the tumors were located unilaterally on the side of the upper half of the medulla oblongata (Figs. 2, 5 and 6, right). One patient (case 1), treated with a lateral approach, showed no further dysfunction except for temporary postoperative impairment of swallowing. The other patient (case 2), treated with an approach to the medial side, experienced postoperative neurological deterioration and sleep apnea. Although sleep apnea occurred postoperatively, a unilateral approach into the medulla oblongata should not cause fatal dysfunction. We were able to distinguish the tumour tissue from adjacent brain by its intraoperative microscopic color and consistency and follow a distinct dissection plane defining the tumor borders. Gross total tumours removal was achieved in both cases by retracting the mass from the surrounding medullary tissue with a two-pronged hook or a small spoon retractor.[49]

## CONCLUSIONS

The medulla oblongata is the most critical area in the brainstem and surgical intervention in this area runs the risk of serious morbidity or mortality. However, one side of the medulla oblongata may be amenable to direct surgery. Although the upper half

of the medulla oblongata is more critical than the lower, a lateral approach to the upper half of the medulla oblongata may result in less morbidity than a medial approach, which has the potential to cause severe or fatal dysfunction. Some cases of focal malignant gliomas in the brainstem may be amenable to gross total removal with an improved outcome. Surgery is indicated when a tumor is located unilaterally and its margin is relatively clear on magnetic resonance images. However, surgical resectability depends primarily on intraoperative cleavage planes. Radical removal is feasible when a plane can be established between the tumor and surrounding medullary tissue.

## REFERENCES


1. Bricolo A, Turazzi S, Cristofori L, Talacchi A. Direct surgery for brainstem tumours. Acta Neurochir Suppl 1991; 53: 148–158.
2. Cantore G, Missori P, Santoro A. Cavernous angiomas of the brain stem. Intra-axial anatomical pitfalls and surgical strategies. Surg Neurol 1999; 52: 84–94.
3. Epstein F, McCleary EL. Intrinsic brain-stem tumors of childhood: surgical indications. J Neurosurg 1986; 64: 11–15.
4. Epstein F, Wisoff J. Intra-axial tumors of the cervicomedullary junction. J Neurosurg 1987; 67: 483–487.
5. Epstein F, Wisoff JH. Intrinsic brainstem tumors in childhood: surgical indications. J Neurooncol 1988; 6: 309–317.
6. Heffez DS, Zinreich SJ, Long DM. Surgical resection of intrinsic brain stem lesions: an overview. Neurosurgery 1990; 27: 789–798.
7. Kyoshima K, Kobayashi S, Gibo H, Kuroyanagi T. A study of safe entry zones via the floor of the fourth ventricle for brain-stem lesions. Report of three cases. J Neurosurg 1993; 78: 987–993.
8. Sindou M, Yada J, Salord F. Functional results after microsurgical resection of brain stem cavernous malformations (retrospective study of a 12 patient series and review of the recent literature). Acta Neurochir 2000; 142: 843–852.
9. Albright AL, Guthkelch AN, Packer RJ, Price RA, Rourke LB. Prognostic factors in pediatric brain-stem gliomas. J Neurosurg 1986; 65: 751–755.
10. Albright AL, Price RA, Guthkelch AN. Brain stem gliomas of children. A clinicopathological study. Cancer 1983; 52: 2313–2319.
11. Alvisi C, Cerisoli M, Maccheroni ME. Long-term results of surgically treated brainstem gliomas. Acta Neurochir 1985; 76: 12–17.
12. Behnke J, Christen HJ, Mursch K, Markakis E. Intra-axial endophytic tumors in the pons and/or medulla oblongata. II. Intraoperative findings, postoperative results, and 2-year follow up in 25 children. Childs Nerv Syst 1997; 13: 135–146.
13. Cohen ME, Duffner PK, Heffner RR, Lacey DJ, Brecher M. Prognostic factors in brainstem gliomas. Neurology 1986; 36: 602–605.
14. Fasano VA, Urciuoli R, Ponzio RM, Lanotte MM. The effects of new technologies on the surgical management of brainstem tumors. Surg Neurol 1986; 25: 219–226.
15. Hoffman HJ. Dorsally exophytic brain stem tumors and midbrain tumors. Pediatr Neurosurg 1996; 24: 256–262.
16. Hoffman HJ, Becker L, Craven MA. A clinically and pathologically distinct group of benign brain stem gliomas. Neurosurgery 1980; 7: 243–248.
17. Jelsma RK, Jelsma LF, Johnson GS. Surgical removal of brainstem astrocytomas and hemangioblastomas: report of three cases and review. Surg Neurol 1993; 39: 494–510.
18. Kansal S, Jindal A, Mahapatra AK. Brain stem glioma-a study of 111 patients. Indian J Cancer 1999; 36: 99–108.
19. Pierre-Kahn A, Hirsch JF, Vinchon M et al. Surgical management of brain-stem tumors in children: results and statistical analysis of 75 cases. J Neurosurg 1993; 79: 845–852.
20. Pollack IF, Hoffman HJ, Humphreys RP, Becker L. The long-term outcome after surgical treatment of dorsally exophytic brain-stem gliomas. J Neurosurg 1993; 78: 859–863.
21. Stroink AR, Hoffman HJ, Hendrick EB, Humphreys RP. Diagnosis and management of pediatric brain-stem gliomas. J Neurosurg 1986; 65: 745–750.
22. Stroink AR, Hoffman HJ, Hendrick EB, Humphreys RP, Davidson G. Transependymal benign dorsally exophytic brain stem gliomas in childhood: diagnosis and treatment recommendations. Neurosurgery 1987; 20: 439–444.
23. Takasato Y, Arai T, Ohta Y, Yamada K. Gross total removal of adult brainstem glioma-two case reports. Neurol Med Chir (Tokyo) 1993; 33: 625–629.
24. Tomita T, McLone DG, Naidich TP. Brain stem gliomas in childhood. Rational approach and treatment. J Neurooncol 1984; 2: 117–122.
25. Vandertop WP, Hoffman HJ, Drake JM et al. Focal midbrain tumors in children. Neurosurgery 1992; 31: 186–194.
26. Xu Q, Bao W, Mao R. Diagnosis and treatment of solid brainstem tumors in adults. Chin Med J (Engl) 1997; 110: 109–113.
27. Abbott R, Shiminski-Maher T, Wisoff JH, Epstein FJ. Intrinsic tumors of the medulla: surgical complications. Pediatr Neurosurg 1991; 17: 239–244.
28. Mantravadi RV, Phatak R, Bellur S, Liebner EJ, Haas R. Brain stem gliomas: an autopsy study of 25 cases. Cancer 1982; 49: 1294–1296.
29. Maria BL, Rehder K, Eskin TA et al. Brainstem glioma: I. Pathology, clinical features, and therapy. J Child Neurol 1993; 8: 112–128.
30. Nishio S, Fukui M, Tateishi J. Brain stem gliomas: a clinicopathological analysis of 23 histologically proven cases. J Neurooncol 1988; 6: 245–250.
31. Selvapandian S, Rajshekhar V, Chandy MJ. Brainstem glioma: comparative study of clinico-radiological presentation, pathology and outcome in children and adults. Acta Neurochir 1999; 141: 721–726.
32. Tokuriki Y, Handa H, Yamashita J, Okumura T, Paine JT. Brainstem glioma: an analysis of 85 cases. Acta Neurochir 1986; 79: 67–73.
33. Edwards MS, Wara WM, Ciricillo SF, Barkovich AJ. Focal brain-stem astrocytomas causing symptoms of involvement of the facial nerve nucleus: long-term survival in six pediatric cases. J Neurosurg 1994; 80: 20–25.
34. Hara M, Takeuchi K. A temporal study of survival of patients with pontine gliomas. J Neurol 1977; 216: 189–196.
35. Lassiter KR, Alexander Jr E, Davis Jr CH, Kelly Jr DL. Surgical treatment of brain stem gliomas. J Neurosurg 1971; 34: 719–725.
36. Littman P, Jarrett P, Bilaniuk LT et al. Pediatric brain stem gliomas. Cancer 1980; 45: 2787–2792.
37. Panitch HS, Berg BO. Brain stem tumors of childhood and adolescence. Am J Dis Child 1970; 119: 465–472.
38. Sanford RA, Freeman CR, Burger P, Cohen ME. Prognostic criteria for experimental protocols in pediatric brainstem gliomas. Surg Neurol 1988; 30: 276–280.
39. Berger MS, Edwards MS, LaMasters D, Davis RL, Wilson CB. Pediatric brain stem tumors: radiographic, pathological, and clinical correlations. Neurosurgery 1983; 12: 298–302.
40. Edwards MS, Prados M. Current management of brain stem gliomas. Pediatr Neurosci 1987; 13: 309–315.
41. Farwell JR, Dohrmann GJ, Flannery JT. Central nervous system tumors in children. Cancer 1977; 40: 3123–3132.
42. Jenkin RD, Boesel C, Ertel I et al. Brain-stem tumors in childhood: a prospective randomized trial of irradiation with and without adjuvant CCNU, VCR, and prednisone. A report of the Childrens Cancer Study Group. J Neurosurg 1987; 66: 227–233.
43. Schulz-Ertner D, Debus J, Lohr F, Frank C, Hoss A, Wannenmacher M. Fractionated stereotactic conformal radiation therapy of brain stem gliomas: outcome and prognostic factors. Radiother Oncol 2000; 57: 215–223.
44. Eifel PJ, Cassady JR, Belli JA. Radiation therapy of tumors of the brainstem and midbrain in children: experience of the Joint Center for Radiation Therapy and Children's Hospital Medical Center (1971–1981). Int J Radiat Oncol Biol Phys 1987; 13: 847–852.
45. Strange P, Wohlert L. Primary brain stem tumours. Acta Neurochir 1982; 62: 219–232.
46. Bilaniuk LT, Zimmerman RA, Littman P et al. Computed tomography of brain stem gliomas in children. Radiology 1980; 134: 89–95.
47. Golden GS, Ghatak NR, Hirano A, French JH. Malignant glioma of the brain-stem. A clinicopathological analysis of 13 cases. J Neurol Neurosurg Psychiatry 1972; 35: 732–738.
48. Duus P. In: Book Topcal Diagnosis in Neurology, Anatomy, Physiology, Signs, Symptoms. New York: Georg Thieme Verlag; 1983.
49. Kyoshima K, Hongo K, Kobayashi S. Spoon retractors for soft mass. J Clin Neurosci 2000; 7: 328–329.


# Identical cerebral aneurysms in siblings: report of two families


**Pablo Hager[1,2], Hans-Jakob Steiger[1,2]**

[1]Department of Neurosurgery, University Hospital, Berne, Switzerland,
[2]Department of Neurosurgery, Ludwig-Maximilians-University, Munich 81377, Germany



**Summary** Two pairs of sisters with identical cerebral aneurysms are reported. In the first family, a sibship of three, the two female members presented with subarachnoid haemorrhages from identical, left internal carotid artery bifurcation aneurysms. The subarachnoid

THE JOURNAL OF BIOLOGICAL CHEMISTRY
Vol. 279, No. 4, Issue of January 23, pp. 3058–3067, 2004
Printed in U.S.A.


# Core 2 Branching β1,6-*N*-Acetylglucosaminyltransferase and High Endothelial Venule-restricted Sulfotransferase Collaboratively Control Lymphocyte Homing*

Received for publication, October 10, 2003, and in revised form, October 28, 2003
Published, JBC Papers in Press, October 30, 2003, DOI 10.1074/jbc.M311150200

**Nobuyoshi Hiraoka‡§, Hiroto Kawashima‡§, Bronislawa Petryniak¶, Jun Nakayama‖, Junya Mitoma‡, Jamey D. Marth**, John B. Lowe¶, and Minoru Fukuda‡ ‡‡**

*From the ‡Glycobiology Program, Cancer Research Center, The Burnham Institute, La Jolla, California 92037, the ¶Howard Hughes Medical Institute, Department of Pathology, The University of Michigan Medical School, Ann Arbor, Michigan 48109, the ‖Department of Pathology, Shinshu University School of Medicine, Matsumoto 390-8621, Japan, and the **Howard Hughes Medical Institute, Division of Cellular and Molecular Medicine, University of California, San Diego, La Jolla, California 92093*

**L-selectin mediates lymphocyte homing by facilitating lymphocyte adhesion to carbohydrate ligands expressed on high endothelial venules (HEV) of the secondary lymphoid organs. Previous studies demonstrated that L-selectin ligand sulfotransferase (LSST) forms 6-sulfo sialyl Lewis x (sLe$^x$) on both core 2 branch and MECA-79-positive extended core 1 *O*-glycans, but the chemical nature and roles of HEV ligands elaborated by LSST and core 2 β1,6-*N*-acetylglucosaminyltransferase-1 (Core2GlcNAcT) have been undefined. In the present study, we have generated mutant mice with deficient LSST and show that inactivation of LSST gene alone leads to only partial impairment of lymphocyte homing to peripheral lymph nodes and moderate reduction in lymphocyte counts in the peripheral lymph nodes, despite the fact that L-selectin ligands that contain 6-sulfo sLe$^x$ are reduced at HEV. By contrast, LSST/Core2GlcNAcT double null mice exhibited a markedly reduced lymphocyte homing and reduced lymphocyte counts as a result of significantly decreased 6-sulfo sLe$^x$ on HEV L-selectin counterreceptors, relative to LSST- or Core2GlcNAcT-single null mice. Moreover, induction of LSST and Core2GlcNAcT transcripts was observed in HEV-like structure formed in the salivary gland of the non-obese diabetic mouse, which displays chronic inflammation. These results indicate that LSST and Core2GlcNAcT cooperatively synthesize HEV-specific L-selectin ligands required for lymphocyte homing and suggest that LSST and Core2GlcNAcT play a critical role in lymphocyte trafficking during chronic inflammation.**

Lymphocyte recirculation through lymph nodes and Peyer's patches is important for detection of foreign antigens by the immune system and subsequent processes that neutralize these molecules. Lymphocyte recirculation critically depends on interaction between the leukocyte adhesion molecule L-selectin and counterreceptors restricted on specialized post capillary venules, high endothelial venules (HEV)[1] in secondary lymphoid organs. The counterreceptors on the luminal surface of HEV capture circulating lymphocytes via L-selectin-dependent adhesive interactions that lead, in turn, to lymphocyte tethering and rolling, chemokine-dependent activation, integrin-mediated firm attachment, and lymphocyte transmigration (1–4). L-selectin and its ligands are also implicated in lymphocyte recruitment in certain chronic inflammation. HEV-like microvasculature is induced on endothelium in association with insulitis characteristic of the non-obese diabetic (NOD) mouse and the rejection of heart transplants in rodents and humans (5–8). Similarly, HEV-like structure is observed in inflammatory bowel diseases, rheumatoid arthritis, lymphocytic thyroiditis, and the hyperplastic thymus of the AKR mouse (9–12). It has been suggested that recruitment of lymphocytes by induced L-selectin ligand may contribute to the pathogenesis of these diseases, which is characteristic of induced HEV-like microvasculature.

L-selectin present on leukocytes is a carbohydrate-binding protein characterized by dependence on $Ca^{2+}$ for its activity. HEV-borne L-selectin counterreceptors include GlyCAM-1, CD34, podocalyxin, Sgp200, endoglycan, and MAdCAM-1, all of which have mucin-like domains that act as scaffolding for *O*-linked oligosaccharides (13). The function of these L-selectin counterreceptors entirely depends on their decoration with specific sialylated, fucosylated, and sulfated oligosaccharides, which contain 6-sulfo sialyl Lewis X (sLe$^x$), (NeuNAcα2→3Galβ1→4[Fucα1→3(sulfo→6)]GlcNAcβ1→R) (14–17). Indeed, recent studies demonstrate that mouse and human L-selectin ligand sulfotransferase (LSST, also known as HEC-GlcNAc6ST or GlcNAc6ST-2 (18)) is capable of forming 6-sulfo sLe$^x$ on core 2-branched *O*-glycans (16, 19). More recent studies demonstrated that LSST together with core 1 extension enzyme (Core1-β3GlcNAcT) forms the MECA-79 epitope, defined as Galβ1→4(sulfo→6)GlcNAcβ1→3Galβ1→3GalNAcα1→R, which is a partial structure of 6-sulfo sLe$^x$ on extended core 1 *O*-glycans (20). The MECA-79 antibody also binds to 6-sulfo sLe$^x$ on extended core 1 and inhibits both *in*

* The work was supported by Grants PO1CA71932 (to M. F. and J. B. L.), DK48247 (to J. D. M.), and R37CA33000 (to M. F.) from the National Institutes of Health, by Howard Hughes Investigator Awards (to J. B. L. and J. D. M.), and by Priority Area 14082201 (to J. N.) from the Ministry of Education, Culture, Sports, Science and Technology of Japan. The costs of publication of this article were defrayed in part by the payment of page charges. This article must therefore be hereby marked "*advertisement*" in accordance with 18 U.S.C. Section 1734 solely to indicate this fact.

§ Both authors equally contributed to the work.

‡‡ To whom correspondence should be addressed: The Burnham Institute, 10901 North Torrey Pines Rd., La Jolla, CA 92037. Tel.: 858-646-3144; Fax: 858-646-3193; E-mail: minoru@burnham.org.

[1] The abbreviations used are: HEV, high endothelial venule; LSST, L-selectin ligand sulfotransferase; Core2GlcNAcT, β1,6-*N*-acetylglucosaminyltransferase-1; Core1-β3GlcNAcT, core 1 extension β1,3-*N*-acetylglucosaminyltransferase; sLe$^x$, sialyl Lewis x; NOD, non-obese diabetic; EGFP; enhanced green fluorescent protein; CMFDA, 5-chloromethyl fluorescence diacetate; GlcNAc6ST-1, GlcNAc-6-*O*-sulfotransferase-1; HPLC, high performance liquid chromatography; ES cells, embryonic stem cells.

*vivo* and *ex vivo* lymphocyte attachment to HEV by neutralizing L-selectin ligands (20, 21). Significantly, 6-sulfo sLe$^x$ on either extended core 1 (20)- or core 2-branched *O*-glycans provides greater L-selectin-dependent cell adhesion under shear force than does 6-sulfo sLe$^x$ on *N*-glycans (16, 20, 22). Moreover, 6-sulfo sLe$^x$ on bi-antennary *O*-glycans containing both core 2 branch and core 1 extension yield more efficient L-selectin-dependent cell adhesion than 6-sulfo sLe$^x$ on core 2 branch or core 1 extension alone, indicating a synergistic effect of bivalent ligands on L-selectin-mediated adhesion (20).

Gene inactivation of LSST through homologous recombination results in significant reduction in lymphocyte homing and loss of MECA-79 at the luminal side of HEV. LSST null (LSST$^\Delta$) mice, however, still exhibit slightly over 50% of lymphocyte homing to the peripheral lymph nodes relative to wild-type mice (23; our results shown below). These observations thus indicate that 6-sulfo sLe$^x$ on extended core 1 *O*-glycans is almost absent in LSST null mice, but 6-sulfo sLe$^x$ on other structures remaining after inactivation of LSST must play a role as L-selectin ligands. One of those ligands is likely to be 6-sulfo sLe$^x$ on core 2-branched *O*-glycans (16, 20). The formation of 6-sulfo sLe$^x$ on core 2-branched *O*-glycans requires core 2 β1,6-*N*-acetylglucosaminyltransferase-I (Core2GlcNAcT) (24). In Core2GlcNAcT null (Core2GlcNAcT$^\Delta$) mice established previously, L-, P-, or E-selectin ligand on neutrophils was significantly diminished. Concomitantly, neutrophil recruitment to inflamed peritoneum in Core2GlcNAcT$^\Delta$ mice was diminished to 20% of levels seen in wild-type mice (25). However, the same studies showed that Core2GlcNAcT$^\Delta$ mice exhibited only partial reduction in lymphocyte homing and lymphocyte counts in the peripheral lymph nodes. Analysis of *O*-glycans remaining after Core2GlcNAcT inactivation demonstrated that no core 2-branched *O*-glycans was detected in GlyCAM-1 isolated from HEV and that the majority of *O*-glycans contains core 1 extension in HEV of Core2GlcNAcT$^\Delta$ mice (20). These results suggest that almost all of the 6-sulfo sLe$^x$ on L-selectin counterreceptors reside either on core 2-branch or extended core 1 *O*-glycans. However, precise structures of these *O*-glycans and their roles in lymphocyte homing have remained undefined.

To determine the roles of LSST and Core2GlcNAcT in L-selectin ligand biosynthesis at HEV, we first generated mutant mice deficient in LSST and then generated double knockout mice deficient in both LSST and Core2GlcNAcT by cross-breeding LSST$^\Delta$ mice with Core2GlcNAcT$^\Delta$ mice, which had been previously established (25). Double knockout mice deficient in both LSST and Core2GlcNAcT exhibited significantly reduced lymphocyte homing activity and lymphocyte numbers in the peripheral lymph nodes, compared with single knockout LSST$^\Delta$ or Core2GlcNAcT$^\Delta$ mice, or to wild-type mice. In addition, LSST and Core2GlcNAcT transcripts were detected in HEV-like microvaculate endothelium formed in the salivary gland of NOD mice. These results together with structural analysis of HEV-derived *O*-glycan ligands demonstrate that LSST and Core2GlcNAcT cooperatively synthesize L-selectin ligands and together play dominant roles in lymphocyte homing and suggest that LSST and Core2GlcNAcT play a critical role in lymphocyte trafficking during chronic inflammation.

## EXPERIMENTAL PROCEDURES

*Generation of Targeted ES Cells*—A genomic fragment of ~25 kb containing mouse LSST gene was isolated from a mouse genomic library as a BAC clone (Research Genetics) and subcloned into pBluescript II SK(−) (Stratagene). To disrupt the enzymatic function of mouse LSST, and to create a fusion protein of enhanced green fluorescent protein (EGFP) with the N terminus of LSST, including the short cytoplasmic domain, transmembrane domain, and stem region, a 1-kb NdeI and BglII segment of the LSST gene encoding the catalytic domain was replaced with a 2-kb fragment carrying EGFP-F and the G418 resistance selection (PGKneo) cassette. The inserted EGFP-F segment containing EGFP coding sequences plus the Ras farnesylation signal, and an SV40 poly(A) signal was prepared by amplification of pEGFP-F vector (Clontech), in which the multicloning sites had been deleted by PCR using 5′-TCCATATGTCCGTCCACAGACACCTTATGGTGAGCA-AGGGCGAGGAG-3′ (5′-primer) and 5′-CGGGATCCGCGTTAAGATA-CATTGATGAGTTTG-3′ (3′-primer). The EGFP-F and PGKneo cassette was flanked by 1 kb of mouse genomic DNA at its 5′ region and by 4.5 kb of mouse genomic DNA at its 3′ region. The targeting vector was linearized and electroporated into R1 ES cells. ES cells were positively selected for G418 resistance and negatively selected by expression of the diphtheria toxin gene, inserted into the targeting vector. Targeting events were identified by PCR amplification with EGFP-specific primer (R1M) and a primer (F1M) specific for a LSST sequence outside the LSST sequence contained in the targeting vector (see Fig. 1*A*). ES cells positively screened by PCR were confirmed by Southern blot analysis using XbaI digestion and the genomic probe A in the 5′ region of homologous recombination (20 kb WT, 10.5 kb mutant) and EcoRV digestion and genomic probe B in the 3′ arm of the LSST genome using the targeting vector (30 kb WT, 5 kb mutant).

*Generation of LSSTΔ Mice and LSST$^\Delta$/Core2GlcNAcT$^\Delta$ Mice*—Chimeric males were produced by injection of LSST$^{+/-}$ ES cells into blastocysts and were bred with C57BL/6 females to produce F1 heterozygotes. Germ line transmission was confirmed by PCR, and LSST$^{+/-}$ progeny were backcrossed onto C57BL/6 wild-type mice. Heterozygous males and females were mated to produce wild-type, heterozygous, and homozygous mutant animals. For PCR analysis to genotype the mice, genomic DNA was purified from mouse tail and used as template. F1M and R1M primer pairs were used for detection of the mutated allele. For detection of the wild-type allele, F1W and R1W were used (see Fig. 1*A*). In some analyses, the following PCR primers were used for simultaneous detection of wild-type and mutant alleles in the same PCR reaction; 5′-AAGAAAGGGAGGCTGCTGATGTTC-3′ (F2W) was used as the 5′-primer and 5′-TCCACCATATCAAAGGGCTGCTGA-3′ (R2W) and R1M as 3′-primers. LSST$^\Delta$ mice were back-crossed with C57BL/6 for a total of three generations. C57BL/6 Core2GlcNAcT$^\Delta$ mice and C57BL/6 LSST$^\Delta$ mice were then bred to generate a C57BL/6 LSST$^\Delta$/Core2GlcNAcT$^\Delta$ strain.

*Detection of LSST-GFP Chimeric Protein and MECA-79 Antigen and Binding of L-selectin-IgM Chimeric Protein to HEV*—The extracellular domain of human L-selectin was amplified by PCR and linked to the DNA sequence encoding for the CH2, CH3, and CH4 domains of human IgM in pcDNA1.1 as described for the mouse L-selectin IgM chimera (26). Binding of L-selectin-IgM was detected by goat biotinylated anti-human IgM antibodies followed by Texas red-conjugated avidin. MECA-79 antigen was detected using MECA-79 antibody (BD Pharmingen (21)), followed by rhodamine-conjugated goat anti-rat IgM. The expression of LSST in HEV was detected by fluorescence derived from LSST-EGFP chimeric protein.

*Isolation of GlyCAM-1*—GlyCAM-1 was prepared from sera of wild-type and LSST$^\Delta$ mice as described previously (27). The samples were subjected to SDS-PAGE, blotted to a nitrocellulose membrane and reacted with anti-GlyCAM-1 antibodies that had been prepared as described previously (27), or MECA-79 antibody followed by goat anti-rabbit immunoglobulins and goat anti-rat IgM antibodies, respectively. The bound antibodies were visualized by ECL (Amersham Biosciences).

*Structural Analysis of Oligosaccharides Attached to GlyCAM-1*—Axillary, cervical, and mesenteric lymph nodes from wild-type, LSST$^\Delta$, Core2GlcNAcT$^\Delta$, or LSST$^\Delta$/Core2GlcNAcT$^\Delta$ mice were metabolically labeled with 0.5 mCi/ml [$^3$H]galactose (20). GlyCAM-1 was purified from the condition medium using a column of anti-GlyCAM-1 antibodies conjugated to UltraLink Biosupport Medium (Pierce), as described previously (27).

*O*-Glycans from the purified GlyCAM-1 were isolated and separated by QAE-Sephadex A-25 column chromatography in 10 mM pyridine-acetate buffer (pH 5.5) before and after removal of sialic acid by mild acid hydrolysis as described previously (20, 28). Monosulfated, disulfated, and trisulfated *O*-glycans, eluted with 70 mM, 120 mM (plus 140 mM), and 250 mM (plus 300 mM) NaCl, respectively, were separately applied to a Bio-Gel P-4 gel filtration column as described previously (16, 20).

Fractionated *O*-glycans were then sequentially treated with α1,3-fucosidase and Jack bean β-galactosidase followed by β-*N*-acetylhexosaminidase B, which cleaves only non-sulfated *N*-acetylglucosamine. After these digestions, the majority of oligosaccharides should yield (sulfo→6)GlcNAcβ1→6(Galβ1→3)GalNAcOH from sulfated core 2-branch *O*-glycans and (sulfo→6)GlcNAcβ1→3Galβ1→3GalNAcOH from sulfated, extended core 1 *O*-glycans, respectively. These two com-

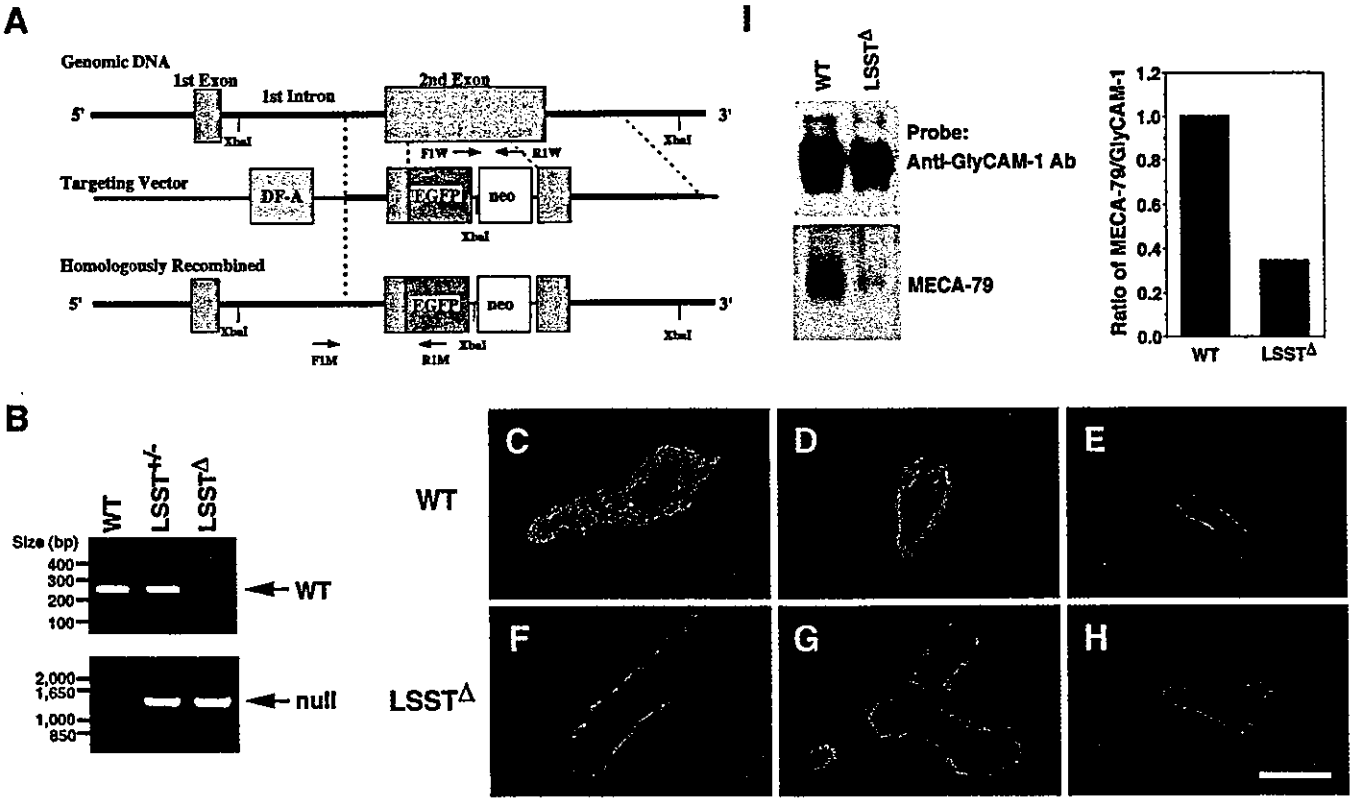


FIG. 1. **Inactivation of the LSST locus.** *A*, structure of wild-type and mutant LSST Loci. The targeting vector replaces the DNA encoding amino acid residues (33–388) of LSST with cDNA encoding EGFP and the herpes virus thymidine kinase cassette (Neo). The targeted allele encodes the cytoplasmic, transmembrane, and stem regions of LSST fused with EGFP under control of the LSST promoter. Diphtheria toxin (*DF-A*) was used for a negative selection. PCR primers are described under "Experimental Procedures." *B*, PCR analysis of genomic DNA derived from wild-type (*WT*) and LSST mutant mice. Using PCR primer sets of F1W/R1W and F1M/R1M (shown in *panel A*). *C–H*, frozen sections of peripheral (*C* and *F*), mesenteric (*D* and *G*), and Peyer's patches (*E* and *H*) from wild-type mice (*C–E*) or from LSST$^{\Delta}$ mice (*F–H*) were examined for L-selectin-IgM chimera binding using fluorescence microscopy. *Bar*, 50 μm. *I*, GlyCAM-1 was prepared from sera of wild-type and LSST$^{\Delta}$ mice, separated by SDS-polyacrylamide gel electrophoresis, and subjected to Western analysis using anti-GlyCAM-1 antibodies or the MECA-79 monoclonal antibody (*left panel*). The *right panel* shows the ratio of MECA-79 over GlyCAM-1, obtained by densitometric analysis of the *left panel*.

pounds can be separated by a shallow gradient elution using a Partisil SAX-10 column (29) or an Asahipak $NH_2$-bonded HPLC column as described previously (20). Oligosaccharides obtained after each step of sequential glycosidase digestion were also fractionated using the Asahipak column. For this, the sample was eluted for 10 min with a linear gradient from solvent A (64% acetonitrile, 36% $H_2O$) to a 70:30 mixture of solvent A and solvent B (64% acetonitrile, 36% 69 mM $NaH_2PO_4/H_2O$, pH 4.2), followed by a 40-min linear gradient elution to a 30:70 mixture of solvent A and solvent B. Finally, the sample was eluted for 5 min with a linear gradient elution to 100% of solvent B. Oligosaccharides were also digested by hexosaminidase A, which cleaves both non-sulfated and sulfated *N*-acetylglucosamine (30). Standard oligosaccharides were prepared from Chinese hamster ovary cells expressing LSST and Core1-β3GlcNAcT or Core2GlcNAcT-I or both.

*Lymphocyte Homing*—Lymphocyte homing *in vivo* was assayed as described previously (26, 31). Briefly, $2.5 \times 10^7$ 5-chloromethyl fluorescein diacetate (CMFDA)-labeled lymphocytes from spleen and mesenteric lymph nodes, derived from wild-type mice, were injected into tail veins of 7- to 8-week-old wild-type, LSST$^{\Delta}$, Core2GlcNAcT$^{\Delta}$, and LSST$^{\Delta}$/Core2GlcNAcT$^{\Delta}$ mice. After 1 h, animals were sacrificed, and peripheral (axillary and cervical) and mesenteric lymph nodes, Peyer's patches, and spleen were isolated. Lymphocyte suspensions were prepared from these organs and subjected to fluorescence-activated cell sorting analysis to determine the fractional content of fluorescent cells.

*Measurement of L-selectin-mediated Rolling on GlyCAM-1 Samples from Wild-type, LSST$^{\Delta}$, Core2GlcNAcT$^{\Delta}$, and LSST$^{\Delta}$/Core2GlcNAcT$^{\Delta}$ Mice*—GlyCAM-1 was prepared from sera of wild-type, LSST$^{\Delta}$, Core2GlcNAcT$^{\Delta}$, and LSST$^{\Delta}$/Core2GlcNAcT$^{\Delta}$ mice, as described above, and captured on polystyrene plates, which had been coated with anti-GlyCAM-1 antibodies (20, 31). The amount of GlyCAM-1 from wild-type, LSST$^{\Delta}$, Core2GlcNAcT$^{\Delta}$, and LSST$^{\Delta}$/Core2GlcNAcT$^{\Delta}$ mice was adjusted to provide equivalent amounts of GlyCAM-1 as assessed by Western blotting analysis using the anti-GlyCAM-1 antibodies. Lymphocytes were initially introduced into the flow chamber at a wall shear stress of 5 dynes/cm$^2$ for 15 s, followed by the termination of flow, allowing cells to adhere under static conditions. Flow rate was then reinitiated at various shear forces. Image analysis was performed and analyzed as described (20, 32). At the same time, rolling velocities for individual cells (between 120 and 200 rolling cells per experiment) were determined for the results obtained on GlyCAM-1 isolated from wild-type and LSST$^{\Delta}$ mice as described previously (16).

*In Situ Hybridization and Immunohistochemistry*—The immunohistochemical staining of MECA-79 antigen and *in situ* hybridization for mouse Core1-β3GlcNAcT, Core2GlcNAcT, LSST, and FucT-VII were performed on the inflamed salivary gland of a 55-week-old NOD mouse as described previously (16, 20). Digoxigenin-labeled antisense and sense RNA probes were prepared by *in vitro* transcription from pGEM-3Zf(+) (Promega) containing a partial cDNA sequence of mouse Core1-β3GlcNAcT (nucleotides +705 to +854), Core2GlcNAcT (nucleotides +991 to + 1140), LSST (nucleotides +556 to +744), or FucT-VII (nucleotides +2196 to + 2497). Hybridized probes were detected by alkaline phosphatase-conjugated anti-digoxigenin antibody, and no specific signals were found in control experiments using sense probes.

Immunohistochemistry with the MECA-79 antibody was performed by the indirect immunoperoxidase method. Control experiments were done by omitting primary antibody from the procedure, and in this case no specific staining was seen. Counterstaining was carried out with hematoxylin.

## RESULTS

*Disruption of the Mouse LSST Locus*—The gene encoding LSST was incorporated into a targeting vector by replacing a portion of the LSST gene with cDNAs encoding EGFP and the neomycin resistance enzyme. After homologous recombination, the resultant gene encodes the cytoplasmic, transmembrane, and stem regions of LSST (amino acid resides 1–32), which are fused with EGFP and driven by the LSST promoter (Fig. 1*A*). It

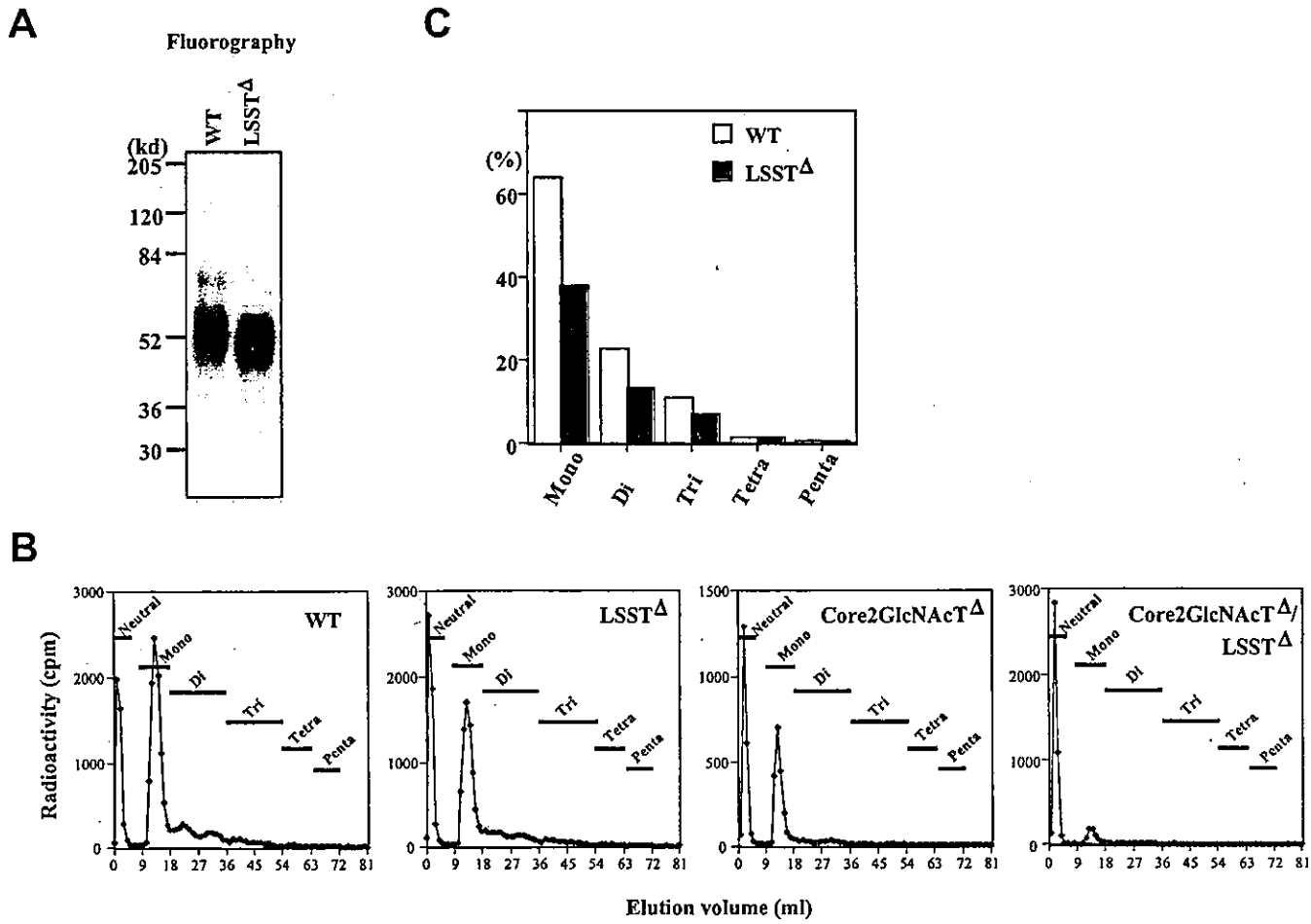


FIG. 2. **Oligosaccharide biosynthesis in LSST-deficient mice.** *A*, GlyCAM-1 purified from the culture medium derived from [$^3$H]galactose labeling of lymph nodes were subjected to SDS-PAGE followed by fluorography. *B*, *O*-linked oligosaccharides were isolated from glycoproteins shown in *panel A* and after removal of sialic acid, subjected to QAE-Sephadex column chromatography. Oligosaccharides eluting at the void volume represent unsulfated *O*-linked oligosaccharides, whereas monosulfated, disulfated, trisulfated, tetrasulfated, and pentasulfated *O*-linked oligosaccharides were eluted by increasing concentrations of NaCl. *C*, the amount of mono-, di-, tri-, tetra-, and pentasulfated *O*-linked oligosaccharides attached to GlyCAM-1 from wild-type and LSST$^{\Delta}$ mice; 100% = total sulfated *O*-linked oligosaccharides of GlyCAM-1 from wild-type mice.

has been shown that the cytoplasmic, transmembrane, and stem regions of Golgi-associated enzymes specify Golgi retention (33, 34), and thus the fused protein is expected to be transported to the same Golgi compartment as the intact LSST.

Targeted ES cell clones were injected into C57BL/6 blastocysts, and F1 crosses of chimeric mice produced LSST$^{\Delta}$ as determined by PCR of genomic DNA (Fig. 1*B*). Intercrosses of heterozygous progeny yielded litters of normal size with Mendelian transmission of the null allele.

*L-selectin Ligand Expression in HEV of LSST$^{\Delta}$ Mice*—LSST$^{\Delta}$ mice did not show a detectable anomaly in the abundance or anatomy of HEV in the secondary lymphoid organs, compared with genetically matched wild-type mice. However, the binding of L-selectin-IgM chimeric protein was almost entirely lost on the luminal side of HEV derived from peripheral and mesenteric lymph nodes under the conditions where strong binding was observed in HEV of wild-type mice (Fig. 1, *C* and *F*). Only a residual binding was detected on the intraluminal surface of the bottom layer of high endothelial cells in LSSTΔ mouse HEV (Fig. 1*F*). However, a more prominent binding of L-selectin-IgM chimeric protein persisted at the bottom layer of high endothelial cells in HEV even after inactivation of LSST (Fig. 1, *F–H*). This layer is called the abluminal lining hereafter. The abluminal expression of L-selectin ligand is also present on Peyer's patches of wild-type mice (Fig. 1*E*). Consistent with these findings, MECA-79 antigen is drastically reduced in GlyCAM-1 isolated from LSST$^{\Delta}$ mice, and only 34% of MECA-79 antigen was detected compared with GlyCAM-1 from wild-type mice (Fig. 1*I*). These results combined strongly suggest that the great majority of 6-sulfo sLe$^x$ on the luminal region of HEV is dependent on LSST, whereas the majority of L-selectin ligand, including 6-sulfo sLe$^x$ in the abluminal lining of lymph nodes and Peyer's patches, is synthesized by a sulfotransferase other than LSST.

*GlyCAM-1 Derived from LSST$^{\Delta}$ Mice Still Contains Significant Amounts of 6-Sulfo sLe$^x$*—The above results suggest that levels of L-selectin ligand in peripheral and mesenteric lymph nodes should be significantly reduced, and only a small fraction of GlyCAM-1 *O*-glycans should contain 6-sulfo sLe$^x$. Because no structural information was available on GlyCAM-1 from LSST$^{\Delta}$ mice in the previous report (23), we analyzed *O*-glycans attached to GlyCAM-1 isolated from peripheral and mesenteric lymph nodes cultured in the presence of [$^3$H]galactose as described previously (Fig. 2*A*) (20). Mucin-type *O*-glycans prepared from the GlyCAM-1 samples of wild-type mice contained a significant amount of sulfated *O*-glycans, which were bound and eluted from a QAE-Sephadex column, whereas appreciable loss of sulfated *O*-glycans was noted for GlyCAM-1 from LSST$^{\Delta}$ mice (Fig. 2*B*).

These oligosaccharides were further analyzed using gel filtration and HPLC as described previously (16, 20). 6-Sulfo sLe$^x$ was reduced in all of GlyCAM-1 *O*-glycans isolated from LSST$^{\Delta}$ mice than wild-type mice (Fig. 2*C*). In particular, 6-sulfo sLe$^x$ in extended core 1 *O*-glycans (shown in *orange* in Fig. 3) is

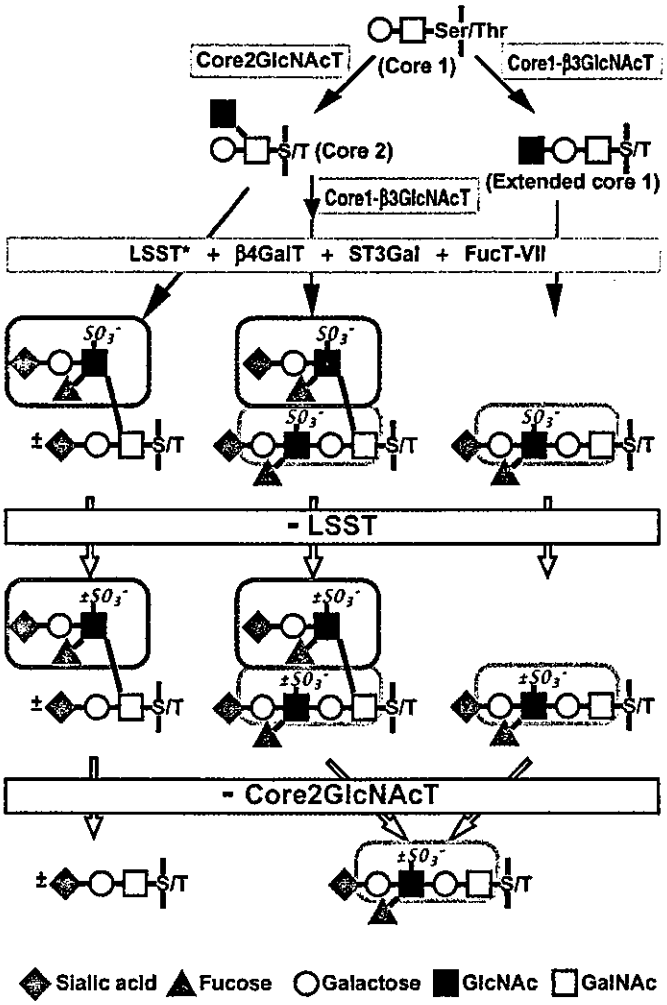


FIG. 3. **Structure and biosynthesis of L-selectin ligand oligosaccharides.** Core 1 *O*-glycan can be extended by Core1-β3GlcNAcT, sulfated by LSST, then galactosylated to form the minimum epitope for the MECA-79 antibody (shown in the *orange circle*). The galactosylated oligosaccharide is further sialylated and fucosylated to form 6-sulfo $sLe^x$ in extended core 1 *O*-glycans (*right*). Core 1 oligosaccharide can be converted to core 2 *O*-glycan by Core2GlcNAcT, sulfated by LSST, galactosylated, sialylated, and fucosylated to form 6-sulfo $sLe^x$ in core 2-branched *O*-glycans (shown in the *magenta circle* at *left*). Core 1-β3GlcNAcT can act on core 2-branched *O*-glycans, leading to biantennary *O*-glycans containing both core 2 branch and core 1 extension. By contrast, Core2GlcNAcT cannot act on extended core 1 *O*-glycans (20). One or both of these branches can be modified to contain 6-sulfo $sLe^x$ (*middle*). All of these processed *O*-glycans function as L-selectin ligands. These schematic structures correspond to *Structure 1* (*left*), *Structure 2* (*right*), and *Structures 3–5* (*middle*) shown in Fig. 5. In addition to LSST, GlcNAc6ST-1 likely forms 6-sulfo *N*-acetylglucosamine in HEV. After inactivation of LSST (*−LSST*), the majority of 6-sulfate in extended core1 is abolished. After further inactivation of Core2GlcNAcT (*−Core2GlcNAcT*), the majority of *O*-glycans is either core 1 *O*-glycans (*bottom left*) or extended core 1 *O*-glycans containing $sLe^x$ (*bottom right*). *β4GalT*, β1,4-galactosyltransferase (52); *ST3Gal*, α2,3-sialyltransferase (53); *FucT-VII*, fucosyltransferase VII.

almost absent (see after inactivation of LSST, *−LSST* in Fig. 3). This finding is consistent with the above finding that the MECA-79 epitope was dramatically diminished in GlyCAM-1 from $LSST^{\Delta}$ mice. Most of the remaining 6-sulfo $sLe^x$ on mucin-type *O*-glycans in HEV was found in core 2-branch (shown in *magenta* in Fig. 3, see below for detailed structural analysis). Core 2 branch in HEV is synthesized exclusively by Core2GlcNAcT (20). These results thus prompted us to generate double knockout mice deficient in both LSST and Core2GlcNAcT to determine the *in vivo* roles of 6-sulfo $sLe^x$ as L-selectin ligands.

*Loss of L-selectin Ligands and 6-Sulfo $sLe^x$ in Double Knockout Mice Deficient in Both LSST and Core2GlcNAcT*—To cross-breed the mice, both LSST null mice and Core2GlcNAcT null mice were separately back-crossed with C57BL/6. Cross-breeding of C57BL/6-$LSST^{\Delta}$ and C57BL/6-$Core2GlcNAcT^{\Delta}$ produced $LSST^{\Delta}$/$Core2GlcNAcT^{\Delta}$ mice with Mendelian transmission of the null allele (Fig. 4*A*). Double knockout mice exhibited no anomalies in gross morphology, were fertile, and were not susceptible to endogenous microbes in a regular pathogen-free environment.

Examination of lymph nodes showed that binding of L-selectin-IgM chimera to HEV was decreased in $Core2GlcNAcT^{\Delta}$ mice, whereas no appreciable loss of MECA-79 antigen was observed (Fig. 4*B*). On the other hand, $LSST^{\Delta}$/$Core2GlcNAcT^{\Delta}$ mice exhibited substantially decreased binding of L-selectin-IgM chimera to HEV and negligible amount of MECA-79 antigen at the luminal side of HEV (Fig. 4*B*). This loss in L-selectin ligand and MECA-79 antigen at the luminal side of the lymph nodes was associated with expression of LSST-GFP protein. These results establish that LSST and Core2GlcNAcT are primarily responsible for L-selectin ligand expression on the luminal side of HEV.

Structural analysis of GlyCAM-1 was carried out to define the chemical nature of the sulfated oligosaccharides. $Core2GlcNAcT^{\Delta}$ mice contained much less sulfated *O*-glycans in GlyCAM-1, which were retained and eluted from a QAE-Sephadex column, than wild-type mice (Fig. 2*B*). Furthermore, a dramatic reduction in sulfated *O*-glycans was observed for GlyCAM-1 derived from $LSST^{\Delta}$/$Core2GlcNAcT^{\Delta}$ mice. The sulfated oligosaccharide fractions isolated by QAE-Sephadex column chromatography were then subjected to Bio-Gel P-4 gel filtration, sequentially digested with specific glycosidases, and analyzed by Bio-Gel P-4 gel filtration and HPLC using an $NH_2$-bonded column as described in previous studies (16, 20). These structural analyses of *O*-glycans derived from wild-type, $LSST^{\Delta}$, $Core2GlcNAcT^{\Delta}$, and $LSST^{\Delta}$/$Core2GlcNAcT^{\Delta}$ mice revealed the oligosaccharide structures shown in Fig. 5*A*. In GlyCAM-1 from wild-type mice, the majority of 6-sulfo $sLe^x$ is contained in core 2-branched *O*-glycans (Fig. 5*A*, *Structure 1*), extended core 1 *O*-glycans (*Structure 2*), monosulfated bi-antennary *O*-glycans (*Structure 3* and *4*), and disulfated bi-antennary *O*-glycans (*Structure 5*) (Fig. 5*A*). In GlyCAM-1 from $LSST^{\Delta}$ mice, MECA-79-positive *Structure 2* is dramatically decreased and MECA-79-positive *Structures 4* and *5* are also decreased. These results are consistent with the above findings that $LSST^{\Delta}$ mice express a negligible amount of luminal MECA-79 antigen. In GlyCAM-1 derived from $Core2GlcNAcT^{\Delta}$ mice, *Structures 1*, *3*, *4*, and *5* containing core 2 branch are absent, whereas MECA-79-positive *Structure 2*, which contains core 1 extension alone, increases (Fig. 5, *A* and *B*).

In GlyCAM-1 derived from $LSST^{\Delta}$/$Core2GlcNAcT^{\Delta}$ double null mice, the amount of oligosaccharides containing 6-sulfo $sLe^x$ in extended core 1 (*Structures 3–5*) is further decreased and only a small amount of *Structure 2* remains, when intraluminal MECA-79 antigen is almost absent (Fig. 4*B*). These results suggest that the majority of MECA-79 antigen in wild-type mice is carried by *Structures 3–5*. At the same time, the amount of non-sulfated $sLe^x$ in $LSST^{\Delta}$/$Core2GlcNAcT^{\Delta}$ mice is increased to 18.7% of total *O*-glycans compared from 11% of those in $Core2GlcNAcT^{\Delta}$ mice (data not shown). These results indicate that the loss of 6-sulfo $sLe^x$ is compensated for by the increase of non-sulfated $sLe^x$ in $LSST^{\Delta}$/$Core2GlcNAcT^{\Delta}$ mice. These results also indicate that LSST is mainly responsible for 6-sulfation at extended core 1 *O*-glycans, whereas a sulfotransferase other than LSST contributes to 6-sulfation at core 2-branch in addition to LSST.

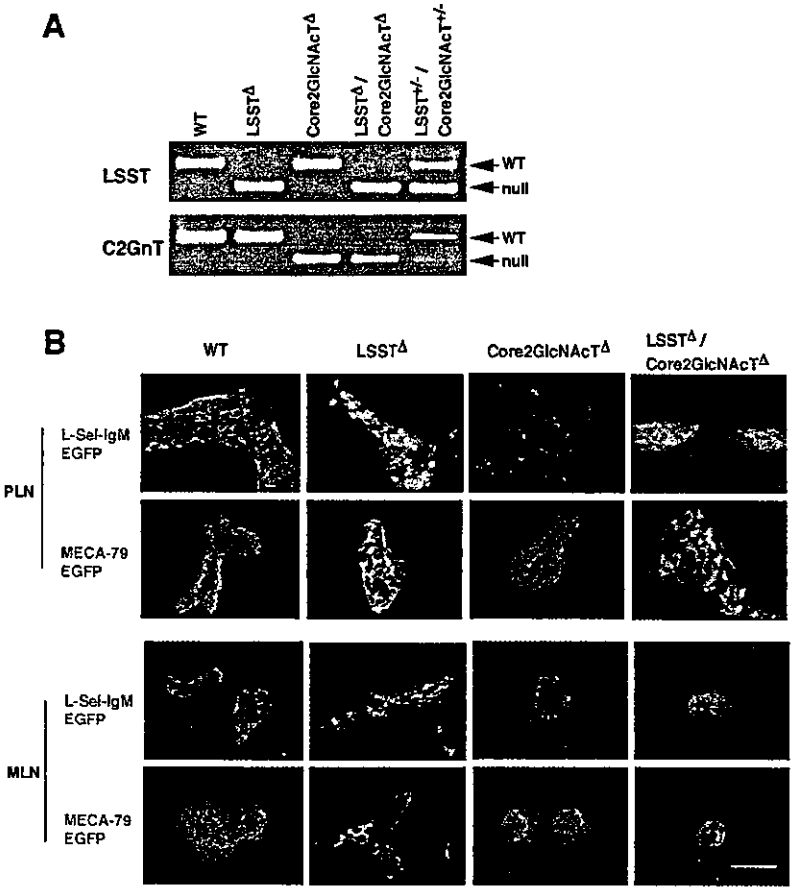


FIG. 4. **Inactivation of both LSST and Core2GlcNAcT.** *A*, cross-breeding of LSST$^{\Delta}$ mice with Core2GlcNAcT$^{\Delta}$ mice. Genomic DNA of mice was analyzed by PCR, which yielded products of correct sizes (479 bp for wild-type (*WT*) and 224 bp for null allele). *B*, expression of L-selectin ligand and MECA-79 antigen in HEV of lymph nodes from wild-type, LSST$^{\Delta}$/Core2GlcNAcT$^{\Delta}$, and LSST$^{\Delta}$/Core2GlcNAcT$^{\Delta}$ mice. Staining is shown for L-selectin-IgM binding or MECA-79 antigen (*red*) and expression of LSST-EGFP (*green*). *PLN*, peripheral lymph nodes; *MLN*, mesenteric lymph nodes. *Bar*, 50 μm.

*Defective Lymphocyte Homing in LSST$^{\Delta}$/Core2GlcNAcT$^{\Delta}$ Mice*—To determine the role of LSST and Core2GlcNAcT in L-selectin ligand activity at HEV, a lymphocyte homing assay was carried out on wild-type, LSST$^{\Delta}$, Core2GlcNAcT$^{\Delta}$, or LSST$^{\Delta}$/Core2GlcNAcT$^{\Delta}$ mice. Homing of wild-type lymphocytes to the peripheral and mesenteric lymph nodes of LSST$^{\Delta}$- or Core2GlcNAcT$^{\Delta}$-recipient mice was decreased to 55 and 85%, respectively, relative to homing in wild-type-recipient mice (Fig. 6*A*). The number of lymphocytes in the peripheral lymph nodes was decreased to 60% in LSST$^{\Delta}$ mice and 78% in Core2GlcNAcT$^{\Delta}$ mice (Fig. 6*B*). By inactivating both LSST and Core2GlcNAcT, a dramatic decrease in lymphocyte homing to peripheral lymph nodes and mesenteric lymph nodes was observed (Fig. 6*A*). The remaining lymphocyte homing activity in the peripheral lymph nodes of LSST$^{\Delta}$/Core2GlcNAcT$^{\Delta}$ mice still depended on L-selectin-mediated adhesion, because anti-L-selectin antibody treatment of lymphocytes completely abolished lymphocyte homing (Fig. 6*A*). This complete inhibition is equivalent to that observed in mice deficient in L-selectin (35) or mice deficient in both FucT-VII and FucT-IV (31). Lymphocyte numbers in the peripheral lymph nodes of double knockout mice were decreased to 40% relative to that of wild-type mice, whereas only a small decrease was observed in lymphocyte numbers in mesenteric lymph nodes of the same mutant mice (Fig. 6*B*). These results in combination suggest that the efficiency of lymphocyte homing is in proportion to the amount of 6-sulfo sLe$^{x}$, regardless of whether 6-sulfo sLe$^{x}$ is present on extended core 1 or core 2 branch structure.

*Loss of 6-Sulfo sLe$^{x}$ Leads to Increase in the Velocity of Rolling Lymphocytes*—To further determine the roles of L-selectin ligands directed by LSST and Core2GlcNAcT, wild-type lymphocytes were rolled over plates that had been coated with GlyCAM-1 prepared from the sera of wild-type, LSST$^{\Delta}$, Core2GlcNAcT$^{\Delta}$, and LSST$^{\Delta}$/Core2GlcNAcT$^{\Delta}$. Surprisingly, GlyCAM-1 from LSST$^{\Delta}$ mice exhibited only a marginal decrease in L-selectin ligand activity compared with wild-type mice (Fig. 6*C*). By contrast, rolling on GlyCAM-1 from Core2GlcNAcT$^{\Delta}$ mice was decreased significantly compared with that seen in wild-type GlyCAM-1. GlyCAM-1 from double knockout LSST$^{\Delta}$/Core2GlcNAcT$^{\Delta}$ mice supported the least amount of lymphocyte rolling (Fig. 6*C*).

The above results suggest, however, that the role of 6-sulfo sLe$^{x}$ was not precisely measured by examining the number of tethering and rolling lymphocytes, because only a marginal decrease was observed on GlyCAM-1 derived from LSST$^{\Delta}$ mice. We thus measured the velocity of rolling lymphocytes, because we previously found that the effect of 6-sulfation on L-selectin ligand is measured best by examining the velocity of rolling lymphocytes (16). GlyCAM-1 from wild-type mice yielded an average velocity of 18 μm/s at a shear stress of 2.32 dyne/cm$^2$, whereas GlyCAM-1 from LSST$^{\Delta}$ yielded ~31 μm/s at the same shear stress (Fig. 6*D*). These results indicate that 6-sulfation on sLe$^{x}$ dramatically decreases the velocity of rolling lymphocytes. By contrast, the number of rolling lymphocytes on LSST$^{\Delta}$ GlyCAM-1 did not decrease at the same shear force and decreased only by 35% under weaker shear forces (Fig. 6*C*). These results suggest that 6-sulfation facilitates lymphocyte homing mainly by decreasing the velocity of rolling lymphocytes.

*Coordinate Expression of LSST, Core2GlcNAcT, Core1-β3GlcNAcT, and FucT-VII in HEV-like Microvasculature of NOD Mice*—L-selectin ligand-positive HEV is constitutively present in secondary lymphoid organs. By contrast, conversion of flat walled vascular endothelium to a HEV-like morphology is observed in association with certain inflammatory and preneoplastic conditions. A well characterized such example, the NOD mouse, displays HEV-like structures in pancreatic islets and inflammatory salivary glands. In these organs, recruitment of lymphocytes through L-selectin ligand leads to β-cell

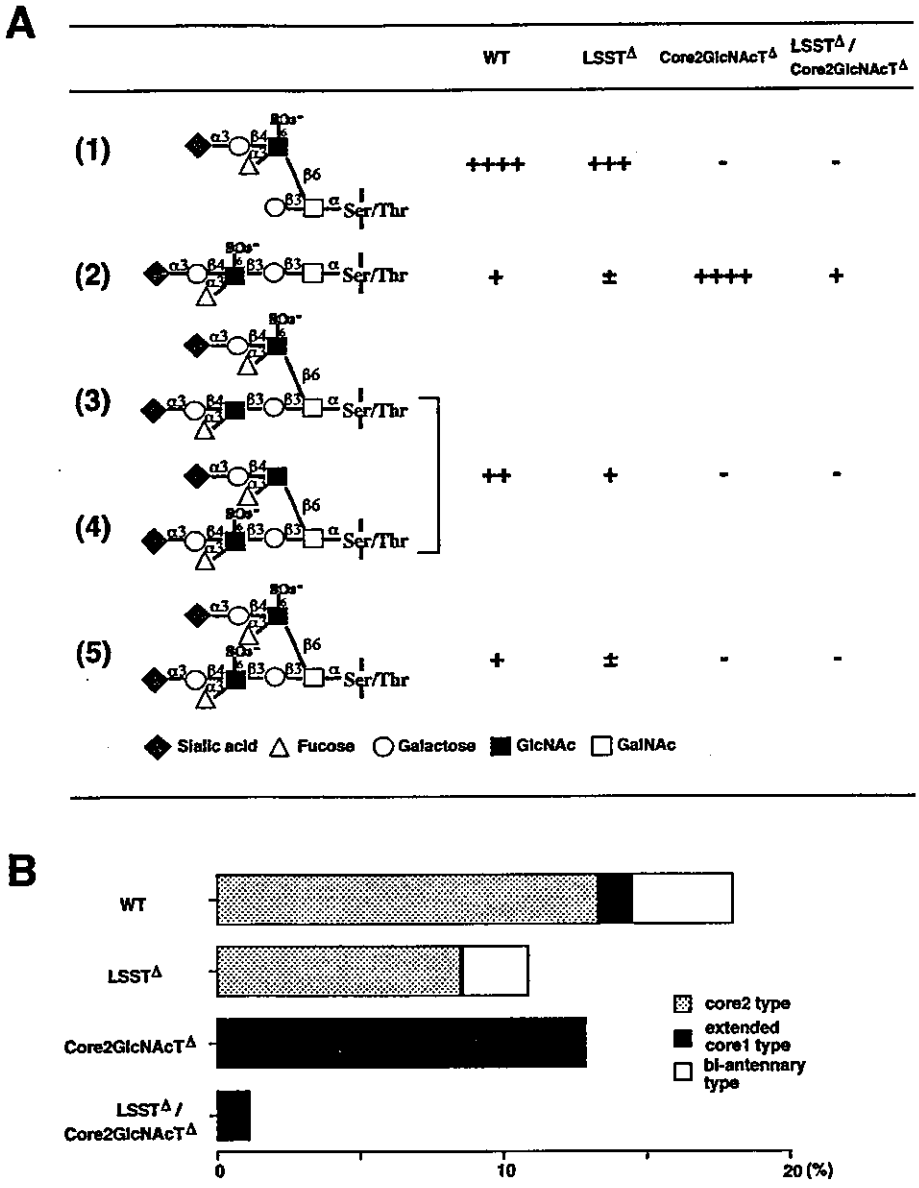


FIG. 5. **Structures of major sulfated *O*-linked oligosaccharides attached to GlyCAM-1 from wild-type, LSST$^{\Delta}$, Core2GlcNAcT$^{\Delta}$, and LSST$^{\Delta}$/Core2GlcNAcT$^{\Delta}$ mice.** *A*, the structures of oligosaccharides containing 6-sulfo sLe$^{x}$ in GlyCAM-1 derived from HEV were determined and shown. *B*, the amount of core 2-branched *O*-glycans (*Structure 1*), extended core 1 *O*-glycans (*Structure 2*), and biantennary *O*-glycans (*Structure 3-5*), which contain 6-sulfo sLe$^{x}$, is shown. 100% = total *O*-glycans that include non-sialylated and non-sulfated *O*-glycans.

destruction and sialoadenitis of salivary glands (5, 6). *In situ* hybridization shows that LSST and Core2GlcNAcT are transcribed in HEV-like MECA-79-positive structures in salivary glands of NOD mice (Fig. 7). These transcripts colocalize in adjacent sections with transcripts for Core1-β3GlcNAcT, FucT-VII, and Core2GlcNAcT, although the expression level of Core2GlcNAcT transcripts is apparently lower than that of the others (Fig. 7). These results imply that LSST, Core1-β3GlcNAcT, FucT-VII, and to a lesser extent Core2GlcNAcT contribute to induction of L-selectin ligands in HEV-like structures present in inflamed salivary glands of the NOD mouse.

## DISCUSSION

Intense interest in the analysis of oligosaccharides elaborated by HEV has been shown in an attempt to understand the role of L-selectin-mediated adhesion in lymphocyte homing. Attempts to answer this question by ablating counterreceptors such as GlyCAM-1 and CD34 have not been useful in defining these oligosaccharides due to the number of highly glycosylated HEV proteins, which carry the same functional oligosaccharides (3, 36). By contrast, deletion of FucT-VII or fucosyltransferase IV (FucT-IV) or their double mutant has yielded useful information indicating an absolute requirement of α1,3-linked fucose for L-selectin ligand activity (26, 31). To define oligosaccharide elements other than fucose, we have inactivated a key sulfotransferase (LSST) that forms 6-sulfo *N*-acetylglucosamine in the context of 6-sulfo sLe$^{x}$, a major ligand for L-selectin. LSST$^{\Delta}$ mice, however, exhibited substantial residual L-selectin ligand activity at HEV, despite the fact that the LSST$^{\Delta}$ mice lost almost all luminal expression of 6-sulfo sLe$^{x}$ in extended core 1 *O*-glycans. These results agree in principle with the previous report on mutant mice deficient in LSST (23). Considering that 6-sulfo sLe$^{x}$ and possibly sLe$^{x}$ on core 2-branched *O*-glycans most likely contribute to the remaining L-selectin ligand activity at HEV, we have generated LSST$^{\Delta}$/Core2GlcNAcT$^{\Delta}$ double null mice by cross-breeding LSST$^{\Delta}$ mice with Core2GlcNAcT$^{\Delta}$ mice. These studies reveal that LSST and Core2GlcNAcT, which form 6-sulfo *N*-acetylglucosamine and core 2-branch, respectively, control L-selectin ligand synthesis in a cooperative manner.

The present study demonstrates that a large portion of L-selectin ligand, 6-sulfo sLe$^{x}$ on HEV, is capped on core 2-branched *O*-glycans. Deletion of Core2GlcNAcT resulted in a significant loss of lymphocyte homing activity and an appreciable decrease in lymphocyte numbers in peripheral lymph

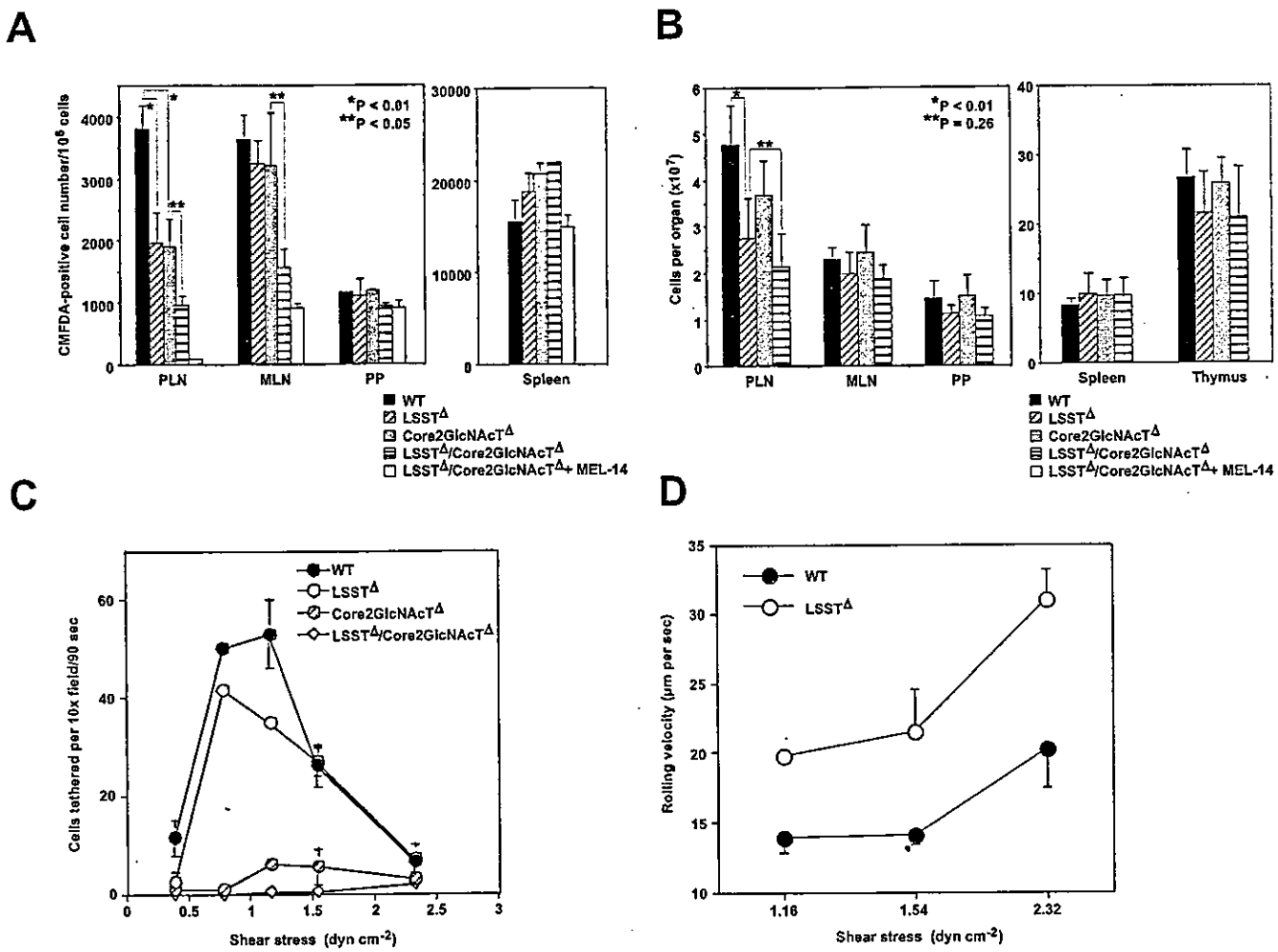


FIG. 6. **Lymphocyte homing and selectin ligand expression in wild-type LSST$^{\Delta}$, Core2GlcNAcT$^{\Delta}$, and LSST$^{\Delta}$/Core2GlcNAcT$^{\Delta}$ mice.** *A*, CMFDA-labeled lymphocytes from mesenteric lymph nodes and spleens of wild-type mice were injected into the tail vein of different mouse strains. Mice were sacrificed 1 h later, and fluorescent lymphocytes in lymphocyte suspensions from lymphoid organs were quantitated by flow cytometry. Residual lymphocyte homing to peripheral lymph nodes in LSST$^{\Delta}$/Core2GlcNAcT$^{\Delta}$ mice was completely abolished by anti-L-selectin antibody (MEL-14) treatment of lymphocytes before the lymphocyte injection. At least four recipient mice were tested for each experiment. *B*, lymphocytes recovered from different lymphoid organs of 7-week-old mice were quantitated. *C* and *D*, lymphocyte rolling using a flow chamber coated with GlyCAM-1 isolated from different strains. The number of adhering lymphocytes is shown for all four mouse strains (*C*), whereas the average rolling velocity of lymphocytes is shown for wild-type and LSST$^{\Delta}$-recipient mice (*D*). In *A–D*, two independent experiments yielded almost identical results and results from one experiment are shown.

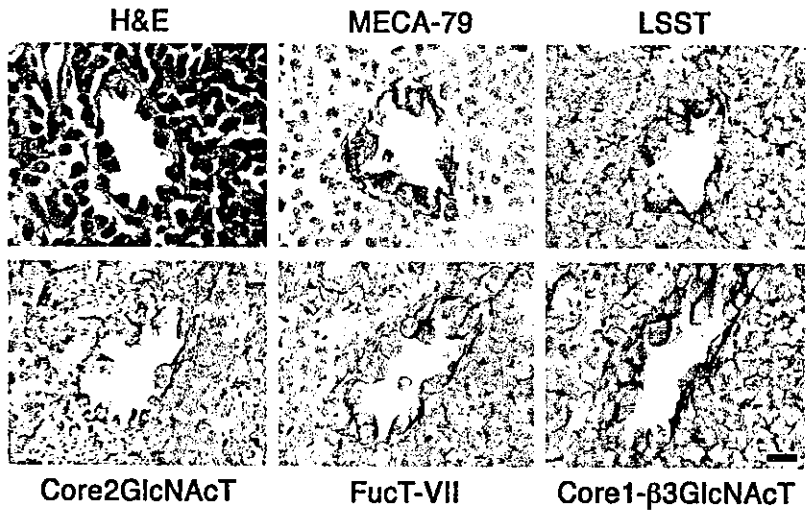


FIG. 7. **Co-localized expression of MECA-79 antigen, LSST, Core2-GlcNAcT, Core1-β3GlcNAcT, and FucT-VII in a HEV-like vessel in the salivary gland of NOD mice.** HEV-like vessels were found in the salivary glands of 55-week-old NOD mice, which developed sialoadenitis accompanying marked lymphocyte infiltration. Serial sections of the representative site were subjected to immunochemistry using the MECA-79 antibody and *in situ* hybridization using antisense probes for mouse LSST, Core2GlcNAcT, FucT-VII, and Core1-β3GlcNAcT. *Bar*, 10 μm.

nodes. These results are, however, slightly different from those obtained in the previous report (25). In the present study, we made efforts to obtain a similar genetic background for LSST$^{\Delta}$ and Core2GlcNAcT$^{\Delta}$ mice by cross-breeding Core2GlcNAcT$^{\Delta}$ and LSST$^{\Delta}$ mice with C57BL/6. Those resultant Core2-GlcNAcT$^{\Delta}$ and LSST$^{\Delta}$ mice were then cross-bred to generate

LSST$^{\Delta}$/Core2GlcNAcT$^{\Delta}$ double knockout mice. For lymphocyte homing assay, lymphocytes from mesenteric lymph nodes and spleen were used in the present study, whereas mesenteric lymphocytes were used in the previous study (25). This difference may cause a different homing profile. In this aspect, it is noteworthy that the previous studies showed a decrement in both lymphocyte homing activity and lymphocyte numbers in the secondary lymphoid organs for Core2GlcNAcT null mice, although it was judged to be statistically insignificant (25). Recently, it has been shown that 6-sulfo sLe$^x$ on bi-antennary *O*-glycans is a better L-selectin ligand than 6-sulfo sLe$^x$ on *O*-glycans containing core 1 extension or core 2-branch alone (20). Core2GlcNAcT$^{\Delta}$ mice entirely lack core 2-branch in HEV L-selectin ligands and such a synergistic effect cannot be achieved in Core2GlcNAcT$^{\Delta}$ mice. This may explain why Core2GlcNAcT$^{\Delta}$ mice exhibit a reduced lymphocyte homing activity relative to wild-type mice.

Stamaa *et al.* (37) reported the presence of 6-sulfo sLe$^x$ on extended core 1 in CD34 isolated from human tonsil. However, the method employed in their study cannot differentiate 6-sulfo sLe$^x$ in extended core 1 *O*-glycan from 6-sulfo sLe$^x$ in core 2-branched *O*-glycan, because no tandem mass spectrometry analysis was performed. Further studies are thus necessary to determine if extended core 1 *O*-glycans (in particular, *Structure 4* in Fig. 5) are present with significant quantity in human tonsil HEV.

Although LSST is concluded to play a critical role in the biosynthesis of 6-sulfo sLe$^x$ at the luminal side of HEV, inactivation of LSST did not lead to loss of L-selectin ligand at the abluminal side of HEV. The abluminal expression of L-selectin ligand and MECA-79 antigen, which constitutes a portion of L-selectin ligand, has been previously reported (21), but has not been studied further. The majority of L-selectin ligand and MECA-79 antigen in the peripheral lymph nodes is strongly expressed on the luminal side of HEV, which has obscured the abluminal L-selectin ligand of the peripheral lymph nodes. However, the abluminal side of Peyer's patches in wild-type mice is also decorated by MECA-79 antigen and L-selectin ligands, which are retained in LSST$^{\Delta}$ mice. In Peyer's patches, it has been shown that L-selectin plays a limited but definite role in the tethering and rolling of lymphocytes, presumably by adhering to L-selectin ligands at the luminal sides of HEV (38, 39). However, this MECA-79-negative L-selectin ligand appears to be relatively weak, because the binding of L-selectin-IgM chimeric protein was not observed at the luminal side of Peyer's patches in both wild-type and LSST$^{\Delta}$ mice (Fig. 1, *E* and *H*). Moreover, L-selectin-mediated lymphocyte homing in Peyer's patches can be compensated with relative ease by other adhesion mechanisms, because anti-L-selectin antibody treatment had a minimum effect on the lymphocyte homing to Peyer's patches (Fig. 6*A*). It is not apparent if this limited role of L-selectin ligand activity on the luminal side of Peyer's patches is supplemented by the presence of abluminal L-selectin ligands.

Our studies also demonstrate that a small amount of 6-sulfo sLe$^x$ is present on extended core 1 *O*-glycans attached to GlyCAM-1 isolated from HEV of LSST$^{\Delta}$/Core2GlcNAcT$^{\Delta}$ mice (Fig. 5*B*). This finding indicates that there must be another sulfotransferase that adds a 6-sulfate group in the context of extended core 1, thus forming the MECA-79 epitope as well. It is also possible that 6-sulfo sLe$^x$ in the abluminal side of HEV after inactivation of LSST may contribute to some of the remaining 6-sulfo sLe$^x$ detected on GlyCAM-1 released from HEV. GlcNAc-6-*O*-sulfotransferase-1 (GlcNAc6ST-1) was shown to form the MECA-79 epitope (40, 41) and thus 6-sulfo sLe$^x$ on extended core 1 *O*-glycans. Because GlcNAc6ST-1 is also expressed in HEV (16, 42), these combined results strongly suggest that GlcNAc6ST-1 also contributes to formation of 6-sulfo sLe$^x$ on HEV in addition to LSST.

The same results also demonstrate that a significant portion of lymphocyte homing to the peripheral lymph nodes remains after inactivation of both LSST and Core2GlcNAcT. This remaining L-selectin ligand activity is apparently more than that expected from residual 6-sulfo sLe$^x$ present in LSST$^{\Delta}$/Core2GlcNAcT$^{\Delta}$ mice. As shown recently, non-sulfated sLe$^x$ on extended core 1 *O*-glycans serves as an L-selectin ligand, although it is not as good a ligand as sLe$^x$ on core 2-branched *O*-glycans (43–45). Because LSST$^{\Delta}$/Core2GlcNAcT$^{\Delta}$ mice contain non-sulfated sLe$^x$ in 18.7% of total *O*-glycans, it is likely that non-sulfated sLe$^x$ on extended core 1 *O*-glycans contributes to this remaining L-selectin ligand. It is also possible that this remaining L-selectin ligand activity may be derived from L-selectin counterreceptors resistant to *O*-glycoprotease (46), which cleaves the majority of glycoproteins that contain mucin type *O*-glycans. This class of MECA-79-negative L-selectin ligand might include heparan sulfate (47, 48) and may play a role in lymphocyte homing.

The transcripts of Core2GlcNAcT and Core1-β3GlcNAcT are expressed in HEV, but they were also detected in wide variety of cells, including colon, lymphocytes, and neutrophils (20, 43, 49, 50). Similarly, the transcripts of FucT-VII are expressed in neutrophils, in addition to HEV (43, 51). In salivary glands of NOD mice, LSST, Core2GlcNAcT, Core1-β3GlcNAcT, and FucT-VII are expressed in HEV-like microvasculature, which is decorated by MECA-79 antigen. Similarly, it was shown that LSST and FucT-VII transcripts were expressed in MECA-79-positive HEV-like microvasculature in hyperplastic thymus of the AKR mouse (16). These observations suggest that LSST, FucT-VII, and in some instances Core1-β3GlcNAcT and Core2GlcNAcT are up-regulated in the formation of HEV and HEV-like structures, and coordinated regulation of these enzymes directs synthesis of L-selectin ligands. The observations on inflamed salivary glands of NOD mice, hyperplastic thymus of AKR mice and HEV in lymph nodes of wild-type mice also suggest that among these enzymes, LSST is most restricted to HEV, and that the up-regulation of LSST may be critical for induction of L-selectin counterreceptors on HEV-like microvasculature in chronic inflammation.

In conclusion, our observations demonstrate that Core2GlcNAcT and HEV-restricted LSST collaboratively control synthesis of L-selectin ligands in HEV. Expression of LSST and Core2GlcNAcT was also observed in HEV-like vasculature formed in inflamed salivary glands of NOD mice. These findings as a whole indicate that LSST and Core2GlcNAcT together provide a major contribution to synthesis of HEV-borne L-selectin ligands, to lymphocyte homing to secondary lymphoid organs, and to lymphocyte trafficking associated with transformation of flat wall vasculature into HEV-like vessels under pathological conditions.

*Acknowledgments*—We thank Dr. Steven Rosen for the kind gift of rabbit anti-GlyCAM-1 antibodies; Drs. Eugene Butcher, James Dennis, and Michiko Fukuda for useful discussions; and Dr. Elise Lamar for organizing the manuscript.

REFERENCES

1. Springer, T. A. (1994) *Cell* **76**, 301–314
2. Butcher, E. C., and Picker, L. J. (1996) *Science* **272**, 60–66
3. Kansas, G. S. (1996) *Blood* **88**, 3259–3287
4. von Andrian, U. H., and Mackay, C. R. (2000) *N. Engl. J. Med.* **343**, 1020–1034
5. Hanninen, A., Taylor, C., Streeter, P. R., Stark, L. S., Sarte, J. M., Shizuru, J. A., Simell, O., and Michie, S. A. (1993) *J. Clin. Invest.* **92**, 2509–2515
6. Faveeuw, C., Gagnerault, M. C., and Lepault, F. (1994) *J. Immunol.* **152**, 5969–5978
7. Turunen, J. P., Majuri, M. L., Seppo, A., Tiisala, S., Paavonen, T., Miyasaka, M., Lemstrom, K., Penttila, L., Renkonen, O., and Renkonen, R. (1995) *J. Exp. Med.* **182**, 1133–1141

8. Toppila, S., Paavonen, T., Nieminen, M. S., Hayry, P., and Renkonen, R. (1999) *Am. J. Pathol.* **155,** 1303–1310
9. Salmi, M., Granfors, K., MacDermott, R., and Jalkanen, S. (1994) *Gastroenterology* **106,** 596–605
10. van Dinther-Janssen, A. C., Pals, S. T., Scheper, R., Breedveld, F., and Meijer, C. J. (1990) *J. Rheumatol.* **17,** 11–17
11. Michie, S. A., Streeter, P. R., Bolt, P. A., Butcher, E. C., and Picker, L. J. (1993) *Am. J. Pathol.* **143,** 1688–1698
12. Michie, S. A., Streeter, P. R., Butcher, E. C., and Rouse, R. V. (1995) *Am. J. Pathol.* **147,** 412–421
13. Rosen, S. D. (1999) *Am. J. Pathol.* **155,** 1013–1020
14. Imai, Y., Lasky, L. A., and Rosen, S. D. (1993) *Nature* **361,** 555–557
15. Hemmerich, S., Leffler, H., and Rosen, S. D. (1995) *J. Biol. Chem.* **270,** 12035–12047
16. Hiraoka, N., Petryniak, B., Nakayama, J., Tsuboi, S., Suzuki, M., Yeh, J. C., Izawa, D., Tanaka, T., Miyasaka, M., Lowe, J. B., and Fukuda, M. (1999) *Immunity* **11,** 79–89
17. Fukuda, M., Hiraoka, N., and Yeh, J. C. (1999) *J. Cell Biol.* **147,** 467–470
18. Fukuda, M., Hiraoka, N., Akama, T. O., and Fukuda, M. N. (2001) *J. Biol. Chem.* **276,** 47747–47750
19. Bistrup, A., Bhakta, S., Lee, J. K., Belov, Y. Y., Gunn, M. D., Zuo, F. R., Huang, C. C., Kannagi, R., Rosen, S. D., and Hemmerich, S. (1999) *J. Cell Biol.* **145,** 899–910
20. Yeh, J. C., Hiraoka, N., Petryniak, B., Nakayama, J., Ellies, L. G., Rabuka, D., Hindsgaul, O., Marth, J. D., Lowe, J. B., and Fukuda, M. (2001) *Cell* **105,** 957–969
21. Streeter, P. R., Rouse, B. T., and Butcher, E. C. (1988) *J. Cell Biol.* **107,** 1853–1862
22. Tangemann, K., Bistrup, A., Hemmerich, S., and Rosen, S. D. (1999) *J. Exp. Med.* **190,** 935–942
23. Hemmerich, S., Bistrup, A., Singer, M. S., van Zante, A., Lee, J. K., Tsay, D., Peters, M., Carminati, J. L., Brennan, T. J., Carver-Moore, K., Leviten, M., Fuentes, M. E., Ruddle, N. H., and Rosen, S. D. (2001) *Immunity* **15,** 237–247
24. Bierhuizen, M. F., and Fukuda, M. (1992) *Proc. Natl. Acad. Sci. U. S. A.* **89,** 9326–9330
25. Ellies, L. G., Tsuboi, S., Petryniak, B., Lowe, J. B., Fukuda, M., and Marth, J. D. (1998) *Immunity* **9,** 881–890
26. Maly, P., Thall, A., Petryniak, B., Rogers, C. E., Smith, P. L., Marks, R. M., Kelly, R. J., Gersten, K. M., Cheng, G., Saunders, T. L., Camper, S. A., Camphausen, R. T., Sullivan, F. X., Isogai, Y., Hindsgaul, O., von Andrian, U. H., and Lowe, J. B. (1996) *Cell* **86,** 643–653
27. Bruehl, R. E., Bertozzi, C. R., and Rosen, S. D. (2000) *J. Biol. Chem.* **275,** 32642–32648
28. Bierhuizen, M. F., Maemura, K., and Fukuda, M. (1994) *J. Biol. Chem.* **269,** 4473–4479
29. Hiraoka, N., Nakagawa, H., Ong, E., Akama, T. O., Fukuda, M. N., and Fukuda, M. (2000) *J. Biol. Chem.* **275,** 20188–20196
30. Kytzia, H. J., and Sandhoff, K. (1985) *J. Biol. Chem.* **260,** 7568–7572
31. Homeister, J. W., Thall, A. D., Petryniak, B., Maly, P., Rogers, C. E., Smith, P. L., Kelly, R. J., Gersten, K. M., Askari, S. W., Cheng, G., Smithson, G., Marks, R. M., Misra, A. K., Hindsgaul, O., von Andrian, U. H., and Lowe, J. B. (2001) *Immunity* **15,** 115–126
32. Finger, E. B., Puri, K. D., Alon, R., Lawrence, M. B., von Andrian, U. H., and Springer, T. A. (1996) *Nature* **379,** 266–269
33. Munro, S. (1991) *EMBO J.* **10,** 3577–3588
34. Aoki, D., Lee, N., Yamaguchi, N., Dubois, C., and Fukuda, M. N. (1992) *Proc. Natl. Acad. Sci. U. S. A.* **89,** 4319–4323
35. Arbones, M. L., Ord, D. C., Ley, K., Ratech, H., Maynard-Curry, C., Otten, G., Capon, D. J., and Tedder, T. F. (1994) *Immunity* **1,** 247–260
36. Suzuki, A., Andrew, D. P., Gonzalo, J. A., Fukumoto, M., Spellberg, J., Hashiyama, M., Takimoto, H., Gerwin, N., Webb, I., Molineux, G., Amakawa, R., Tada, Y., Wakeham, A., Brown, J., McNiece, I., Ley, K., Butcher, E. C., Suda, T., Gutierrez-Ramos, J. C., and Mak, T. W. (1996) *Blood* **87,** 3550–3562
37. Satomaa, T., Renkonen, O., Helin, J., Kirveskari, J., Mäkitie, and Renkonen R. (2002) *Blood* **99,** 2609–2611
38. Bargatze, R. F., Jutila, M. A., and Butcher, E. C. (1995) *Immunity* **3,** 99–108
39. Kunkel, E. J., Ramos, C. L., Steeber, D. A., Muller, W., Wagner, N., Tedder, T. F., and Ley, K. (1998) *J. Immunol.* **161,** 2449–2456
40. Kimura, N., Mitsuoka, C., Kanamori, A., Hiraiwa, N., Uchimura, K., Muramatsu, T., Tamatani, T., Kansas, G. S., and Kannagi, R. (1999) *Proc. Natl. Acad. Sci. U. S. A.* **96,** 4530–4535
41. Uchimura, K., El-Fasakhany, F. M., Hori, M., Hemmerich, S., Blink, S. E., Kansas, G. S., Kanamori, A., Kumamoto, K., Kannagi, R., and Muramatsu, T. (2002) *J. Biol. Chem.* **277,** 3979–3984
42. Uchimura, K., Muramatsu, H., Kadomatsu, K., Fan, Q. W., Kurosawa, N., Mitsuoka, C., Kannagi, R., Habuchi, O., and Muramatsu, T. (1998) *J. Biol. Chem.* **273,** 22577–22583
43. Mitoma, J., Petryniak, B., Hiraoka, N., Yeh, J. C., Lowe, J. B., and Fukuda, M. (2003) *J. Biol. Chem.* **278,** 9953–9961
44. Leppänen, A., Yago, T., Votto, V. I., McEver, R. P., and Cummings, R. D. (2003) *J. Biol. Chem.* **278,** 26391–26400
45. Fieger, C. B., Sassetti, C. M., and Rosen, S. D. (2003) *J. Biol. Chem.* **278,** 27390–27398
46. Clark, R. A., Fuhlbrigge, R. C., and Springer, T. A. (1998) *J. Cell Biol.* **140,** 721–731
47. Wang, L., Brown, J. R., Varki, A., and Esko, J. D. (2002) *J. Clin. Invest.* **110,** 127–136
48. Kawashima, H., Watanabe, N., Hirose, M., Sun, X., Atarashi, K., Kimura, T., Shikata, K., Matsuda, M., Ogawa, D., Heljasvaara, R., Rehn, M., Pihlajaniemi, T., and Miyasaka, M. (2003) *J. Biol. Chem.* **278,** 13069–13076
49. Yeh, J. C., Ong, E., and Fukuda, M. (1999) *J. Biol. Chem.* **274,** 3215–3221
50. Shiraishi, N., Natsume, A., Togayachi, A., Endo, T., Akashima, T., Yamada, Y., Imai, N., Nakagawa, S., Koizumi, S., Sekine, S., Narimatsu, H., and Sasaki, K. (2001) *J. Biol. Chem.* **276,** 3498–3507
51. Smith, P. L., Gersten, K. M., Petryniak, B., Kelly, R. J., Rogers, C., Natsuka, Y., Alford, J. A., III, Scheidegger, E. P., Natsuka, S., and Lowe, J. B. (1996) *J. Biol. Chem.* **271,** 8250–8259
52. Ujita, M., McAuliffe, J., Schwientek, T., Almeida, R., Hindsgaul, O., Clausen, H., and Fukuda, M. (1998) *J. Biol. Chem.* **273,** 34843–34849
53. Priatel, J. J., Chui, D., Hiraoka, N., Simmons, C. J., Richardson, K. B., Page, D. M., Fukuda, M., Varki, N. M., and Marth, J. D. (2000) *Immunity* **12,** 273–283

Available online at www.sciencedirect.com
SCIENCE DIRECT®
Biochemical and Biophysical Research Communications 314 (2004) 1086–1092
BBRC
www.elsevier.com/locate/ybbrc

# Molecular cloning and expression of HRLRRP, a novel heart-restricted leucine-rich repeat protein

Tokio Nakane,[a,*] Toshio Satoh,[a] Yoichi Inada,[a] Jun Nakayama,[b] Fumiaki Itoh,[a] and Shigetoshi Chiba[a]

[a] *Department of Molecular Pharmacology, Shinshu University School of Medicine, Asahi 3-1-1, Matsumoto 390-8621, Japan*
[b] *Department of Pathology, Shinshu University School of Medicine, Asahi 3-1-1, Matsumoto 390-8621, Japan*

Received 22 December 2003

**Abstract**

We isolated a novel leucine-rich repeat protein (LRRP) cDNA from E13 mouse embryos by the in silico approach. The cDNA encoded a protein of 274 amino acids having 7 leucine-rich repeat motifs at the center of the protein. An in vitro transcription/translation study showed that the cDNA coded for a peptide of approximately 31 kDa. Northern blot analysis suggested that the mRNA of this novel LRRP was expressed only in the heart, although RT-PCR indicated slight expression in skeletal muscle as well. The transcripts of this gene and *Nkx-2.5/Csx* were detected in the early stage of cardiac differentiation of P19CL6 embryonal carcinoma cells treated with 1% dimethyl sulfoxide. The fusion protein made between it and GFP was detected at a high level in mitochondria and a low level in the nuclei of COS7 cells. The nuclei of the adult mouse heart were strongly stained with the antibody raised against the synthetic peptide of the protein. Therefore, we designated the gene as heart-restricted leucine-rich repeat protein (HRLRRP) and assume that mouse HRLRRP may play important roles in cardiac development and/or cardiac function.


*Keywords:* Leucine-rich repeat; Heart; Nucleus; Mitochondria; P19 embryonal carcinoma; Differentiation; GFP

The loss of cardiac myocytes caused by ischemic heart diseases and various cardiomyopathies impairs cardiac pump function and leads to heart failure. Recent studies showed that cardiomyocytes divide and grow after myocardial infarction [1], and that bone marrow stem cells and endothelium transplanted into the heart differentiate into cardiac myocytes [2,3]. Many groups have tried to develop novel therapies involving regeneration to form new cardiomyocytes and transplantation of the new cardiomyocytes to the impaired heart. It is important for developing such therapies to unveil the mechanisms of cardiac differentiation and development.

The mechanisms controlling skeletal muscle development have been defined in detail [4], but those of cardiac muscle development are not yet fully understood. Although the roles of transcription factors such as GATA-4, Nkx-2.5/Csx, and MEF-2 have been clarified, forced expression of these transcription factors has never induced cardiac differentiation [5,6]. Therefore, many key genetic regulators of cardiac development remain to be identified.

To identify unknown cardiac-specific genes, homology cloning [7,8], subtractive hybridization [9], differential-display RT-PCR [10], microarray [11], and serial analysis of gene expression (SAGE) [12] have been used. Expressed sequence tag (EST) databases were searched for novel sequences found only in cardiac cDNA libraries, and a novel cardiac-specific gene was cloned [13]. As recent progress made in genome projects has increased the number of EST and full-length cDNA clones in genome databases [14], searching EST databases would be expected to result in the discovery of novel cardiac-specific genes.

We report here the cloning of cDNA encoding a novel mouse heart-restricted leucine-rich repeat protein (HRLRRP) and the expression of its gene in adult mouse tissues and during differentiation of P19CL6 embryonal carcinoma cells to cardiomyocytes [15]. In addition, we describe the results of in vitro transcription/

* Corresponding author. Fax: +81-263-37-3085.
*E-mail address:* nakane@sch.md.shinshu-u.ac.jp (T. Nakane).

0006-291X/$ - see front matter © 2004 Elsevier Inc. All rights reserved.
doi:10.1016/j.bbrc.2003.12.202

translation of the cDNA, the forced expression of it in COS7 cells, and the immunostaining of the adult mouse heart with the antibody raised against the synthetic peptide of the protein.

## Materials and methods

*Cell cultures.* P19CL6 embryonal carcinoma and COS7 cells were obtained from the Riken Cell Bank. P19CL6 cells were cultured in α MEM, and COS7 cells in DMEM, both supplemented with 10% fetal bovine serum (Equitech-Bio) and penicillin/streptomycin. To induce cardiac differentiation, we treated P19CL6 cells were with 1% dimethyl sulfoxide (DMSO) according to Habara-Ohkubo [15].

*Clone selection.* We searched DNA sequence databases (DDBJ and DDBJNEW) by keywords (mouse, embryo, and heart) by using the Sequence Retrieval System of DDBJ. About 20,000 clones were isolated. The homologies of the clones that had not been annotated were analyzed by BLAST in the EST database. We selected the clones that were expressed mainly in the heart.

*Cloning of mouse HRLRRP cDNA.* Poly(A)$^+$ RNA was isolated from ICR mouse (Japan SLC) embryos (E13) by use of a FastTrack kit (Invitrogen). Double-stranded cDNAs were synthesized by a RiboClone cDNA Synthesis System (Promega) using oligo($dT_{16}$) primer. cDNA for HRLRRP was amplified by use of platinum *Taq* polymerase High Fidelity (Invitrogen) and primers: 3882LF (5′-CCACTCCCTGACAGA GTTGGTG-3′) and 3882LR (5′-GCTGGTGGCGTTGTTTTCTTC-3′). The primers used were derived from the sequences of EST clones (AI553065, BB473882, and BB658645) with the aid of the computer program Primer3. The PCR process involved 95 °C for 2 min and 35 cycles of 94 °C for 30 s, 62 °C for 30 s, and 68 °C for 3 min. At the last cycle, PCR products were extended by keeping the temperature at 68 °C for 7 min. The resulting PCR fragment was purified, blunted by $T_4$ DNA polymerase, phosphorylated by $T_4$ polynucleotide kinase, and ligated to the *Sca*I-digested and dephosphorylated pBK-CMV vector (Stratagene) by $T_4$ DNA ligase. The plasmid was sequenced by an autosequencer (Applied Biosystems model 377) using a *Taq* DyeDeoxy Terminator cycle sequencing kit (Perkin–Elmer).

*Total RNA isolation.* Total RNA was isolated from P19CL6 cells and ddY mouse (Japan SLC) tissues by the acid guanidine–phenol–chloroform method of Chomczynski and Sacchi [16] using ISOGEN (Nippon Gene).

*Northern blot analysis.* The cDNA of mouse HRLRRP and the PCR product of mouse G3PDH amplified by G3PDH primers (Clontech) were labeled with biotin by use of a BrightStar Psoralen-Biotin kit (Ambion). Total RNA (15 μg) from each mouse tissue was subjected to 1.2% agarose–formaldehyde gel electrophoresis and subsequently transferred to a BrightStar Plus Positively Charged Nylon Membrane (Ambion). Hybridization and signal detection were carried out by using NorthernMax and BrightStar detection kits (Ambion), respectively.

*RT-PCR.* Mouse total RNA (5 μg) of each organ was treated with DNase I from a DNA-*free* kit (Ambion). RT-PCR was performed with an RNA PCR kit (Perkin–Elmer). Briefly, first-strand cDNA was synthesized from 100 ng of the DNase I-treated RNA by using oligo($dT_{16}$) as a primer and amplified by PCR using Platinum *Taq* polymerase (Invitrogen) instead of *Taq* polymerase. The amplification sequence consisted of an initial denaturation at 95 °C for 2 min, followed by 40 (atrial natriuretic peptide [ANP] and Nkx-2.5/Csx), 42 (HRLRRP), and 36 (β-actin) cycles of 94 °C for 30 s and 60 °C for 30 s. A final extension at 72 °C for 7 min was performed. Contamination by genomic DNA was checked by conducting 50 cycles of the total RNA without reverse transcription by using Nkx-2.5/Csx primers. No PCR product was detected in the reaction mixture lacking reverse transcriptase. The following primers were used 5′-CTCCGAAGGCATCTCATTAG-3′ (3882F2) and 5′-CT GCTTCTGGCACAGGAGTGAC-3′ (3882R2) for HRLRRP; 5′-TAT GCAGAGTGGGAGAGG-3′ (ANPF) and 5′-CTCTGAGAGACGG CAGTGCT-3′ (ANPR) for ANP; 5′-CAGTGGAGCTGGACAAA GCC-3′ (CSXF) and 5′-TAGCGACGGTTCTGGAACCA-3′ (CSXR) for CSX; and 5′-GTGGGAATGGGTCAGAAGGA-3′ (β-actinF) and 5′-CAGGGACAGCACAGCCTGGA-3′ (β-actinR) for β-actin.

*In vitro transcription and translation.* pBK-CMV-HRLRRP was digested by endonucleases *Eco*RI and *Not*I. HRLRRP cDNA was ligated to pcDNA3.1 (Invitrogen) digested by *Eco*RI and *Not*I. In vitro transcription and translation was performed by using a TNT Coupled Reticulocyte Lysate System (Promega) according to the manufacturer's instructions. Briefly, 1 μg of DNA was mixed with 48 μl of a reaction mixture including 1 μl of Transcend tRNA. The reactions were incubated for 90 min at 30 °C. Then 10 μl of the reaction mixture was removed and added to 10 μl of sample buffer. The samples were then heated at 90 °C for 5 min and were analyzed on a 15% SDS–PAGE gel. After electrophoresis, the gel was blotted onto a PVDF membrane by a semidry electroblotter according to the manufacturer's instructions. The signal detection was carried out by using a Transcend Non-Radioactive Translation Detection System kit (Promega).

*Expression in mammalian cells.* pBK-CMV-HRLRRP was amplified by Platinum *Taq* polymerase High Fidelity using 3882prF1 (5′-ATT GGATVVAATGGGAAACACCATCCGGGCCT-3′) and 3882pr-r (5′-ATAGAATTCGAGAGCTGGAAGGAAGAAGGGAG-3′) as primers. The PCR products were digested by *Bam*HI and *Eco*RI. *Bam*HI–*Eco*RI fragments of mouse HRLRRP cDNA were ligated into a pQBI25-fA1 GFP expression vector (Nippon Gene) that had been digested by *Bam*HI and *Eco*RI. For construction of FLAG-tagged protein, pBK-CMV-HPLRRP was amplified by Platinum *Taq* polymerase High Fidelity using primers T3F: (5′-GCCAAGCTCGAAATTAACC CT-3′) and 3882cdsET-r (5′-TAAGGATCCGCAGAGCTGGAAGG AAGAAGG-3′). The PCR product was digested by *Eco*RI and *Bam*HI and then ligated to pFLAG-CMV-5 b (Sigma) that had been digested by *Eco*RI and *Bam*HI. COS7 cells were then transfected with pQBI-HRLRRP and pFLAG-HRLRRP clones by use of FuGENE6 (Roche). After 24 or 48 h, the intracellular location of HRLRRP protein was examined by confocal microscopy (Radiance2100, Bio-Rad). To stain mitochondria and nuclei, we added 500 nM Mitotracker Red CMXRos (Molecular Probes) and 10 μg/ml Hoechst 33342 (Dojindo), respectively, to the culture medium. The cells were incubated at 37 °C for 30 min, washed 3 times with PBS, fixed with 3.7% formaldehyde/PBS, and washed again with PBS 3 times. HRLRRP-FLAG protein was detected by using anti-FLAG M2 antibody (Sigma), as previously described [17].

*Preparation of polyclonal antibody.* Polyclonal antibody for the mouse HRLRRP was generated by immunizing rabbits with keyhole limpet hemocyanin conjugated synthetic peptide selected from deduced amino-acid sequence. Peptide sequence used for generation of an antibody was EPDPRKARRY (amino acids 246–255). The specificity of the antibody was confirmed by Western blotting. COS7 cells were transfected with pME18S-HRLRRP and pFLAG-HRLRRP by use of FuGENE6. After 48 h, COS7 cells were isolated, washed by PBS, and lysed in ice-cold RIPA buffer containing a protease inhibitor cocktail (Sigma). The samples were incubated on ice for 30 min and then centrifuged at 12,000*g* for 15 min at 4 °C. The supernatants were loaded on a 15% SDS–PAGE gel and transferred onto a PVDF membrane as previously described. The membranes were probed with a mouse anti-FLAG M2 monoclonal antibody (Sigma) (1:200) or a rabbit anti-HRLRRP polyclonal antibody, ST1027 (1:800). HRLRRP and HRLRRP-FLAG proteins were detected with a 1:5000 dilution of alkaline phosphatase-conjugated goat anti-rabbit IgG (Fc) antibody and goat anti-mouse IgG (H + L) antibody, respectively. The signal detection was carried out by using a ProtoBlot II AP System with Stabilized Substrate kit (Promega).

*Immunohistochemistry.* Tissue samples including the heart, skeletal muscle, and liver were isolated from male ddY mouse (8 weeks) and immediately frozen in an OCT compound (Sakura Finetek) at −80 °C. Frozen sections sliced at 7-μm thickness were placed on MAS-coated slides (Matsunami Glass), air-dried, and then fixed with 20% formalin

neutral buffer solution (pH7.4) (Wako) for 10 min. After blocking with 1% normal gout serum in 0.05 M Tris buffer (pH 7.6) containing 1% bovine serum albumin, these tissue specimens were incubated with anti-HRLRRP antibody, ST1027 (1:100), overnight at 4 °C. After washing with Tris-buffered saline, they were incubated with goat anti-rabbit IgG conjugated to peroxidase labeled-dextran polymer (EnVision + TM, DAKO) for 1 h at room temperature. The peroxidase reaction was developed with a diaminobenzidine/$H_2O_2$ solution and counter staining was performed with hematoxylin. In control experiments, the preimmune serum was used instead of ST1027 antibody or the primary antibody was omitted from the staining procedure. In both control experiments, no specific staining was found.

*Nucleotide accession number.* The nucleotide sequence data reported in this paper will appear in the DDBJ, EMBL, and GenBank nucleotide sequence databases with Accession No. AB091100.

## Results

### *Cloning of mouse HRLRRP cDNA*

In a homology search using BLAST, an EST clone (the 5′-clone: BB473882 and the 3′-clone: BB658645, the full-length-clone: AK084466) was expressed only in heart cDNA libraries. Thirty-three mouse, rat, pig, and chicken EST clones from embryo, neonate, and adult heart cDNA libraries scored more than 50 bits. BLAST searches in non-redundant databases showed that the nucleic acid sequence of clone AK084466 agreed with those of mRNA clones (AF527781, encoding a mouse putative leucine-rich repeat protein; AK085779, a mouse 16-day neonate heart cDNA clone; XM23516, encoding a rat protein similar to putative leucine-rich repeat protein; and AK123908, *Homo sapiens* cDNA FLJ41914 fis) and genome clones (AL589661, a mouse DNA sequence from clone RP23-58B7 on chromosome 15; AC018921, human 12 BAC RP11-956E11). Therefore, we cloned the gene from the cDNA of mouse E13 embryos by RT-PCR. A PCR product (approximately 1.3 kb) was amplified. The cDNA was 1257 bp in length (Fig. 1A). The longest open reading frame encoded a 274-amino acid polypeptide sequence beginning with the initiation codon at nucleotide position 53 and having a calculated molecular weight of 31,243 Da.

### *Structure of mouse HRLRRP*

Further analysis of the amino acid sequence by using the SMART system revealed the presence of a leucine-rich repeat (LRR) at the center of the peptide (Fig. 1). As shown in Table 1 and Fig. 1B, the protein consisted of 7 repeats; each of 20–23 residues including 7 conserved leucines (or an aliphatic residue) as well as a proline and asparagine. The consensus sequence was **LxxLxxLxL/IxxNxLxxL/FPxxL/Vxx**, where x was any amino acid. The PSORT II program [18] for the prediction of protein localization sites indicated 2 possible nuclear localization signals (residues 247–253 and 249–255), as shown in Fig. 1B.

Table 1

| LRR | Amino acid sequence | Residues | No. of residues |
|---|---|---|---|
| 1 | FTELVKLYLSDNHLHSLPPDLFAQ | 51–73 | 23 |
| 2 | LGRNLQILALDFNNFKALPRVVC | 74–95 | 22 |
| 3 | LKQLCILYLGNNKLCDLPDELFSL | 97–119 | 23 |
| 4 | LQNLRTLWLESNCLTRLPDVVCE | 120–142 | 23 |
| 5 | LSILKTLHAGSNALRLLPGQ | 143–162 | 20 |
| 6 | LRELRTIWLSGNQLADFPSVLLR | 166–188 | 23 |
| 7 | MPFLEVIDVDRNSIRYFPSL | 189–208 | 20 |
| Cons. | LxxLxxLxLxxNxLxxLPxxLxx | | |

*Note.* LRR, leucine-rich repeat; cons., consensus amino acid sequence.

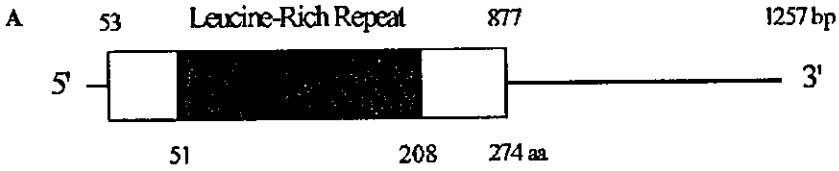


B

```
M G N T I R A F V A F I P T D R C Q S Y V V G D L R E M P L  30
D R M V D L S G S Q L R R F P L H V C S F T E L V K L Y L S  60
D N H L H S L P P D L A Q L Q N L Q I L A L D F N N F K A L  90
P R V V C T L K Q L C I L Y L G N N K L C D L P D E L S L L 120
Q N L R T L W L E S N C L T R L P D V V C E L S L L K T L H 150
A G S N A L R L L P G Q L R R L R E L R T I W L S G N Q L A 180
D F P S V L L R M P F L E V I D V D R N S I R Y F P S L A H 210
L T N L K L V I Y D H N P C R N A P K V G K G V R R V G R W 240
A E E T P E P D P R K A R R Y A L A K E E N Q E P P P P L L 270
P S S S                                   274
```

Fig. 1. Gene structure (A) and deduced amino acid sequence (B) of mouse HPLRRP (GenBank Accession No. AB091100). (B) Underlines, leucine rich-repeat; bold characters, possible nuclear localization signals.

*Northern blot analysis and RT-PCR*

Northern blotting detected an approximately 1.3-kbp HRLRRP transcript, which was found only in the mouse heart (Fig. 2A). RT-PCR for 32 cycles detected HRLRRP mRNA in skeletal muscle, whereas only 24 cycles revealed it in the heart (Fig. 2B). The mRNA was not detected in the other tissues, even after 45 cycles (data not shown). RT-PCR analysis showed that HRLRRP, Nkx-2.5/Csx, and ANP mRNAs were expressed in P19CL6 cells by 2 or 3 days after the DMSO treatment (Fig. 3).

*In vitro transcription and translation*

To determine whether the full-length mouse HRLRRP cDNA encoded the deduced 274-amino acid protein or not, we performed an in vitro transcription/translation assay. In vitro transcription/translation of sense mouse HRLRRP cDNA produced a peptide for approximately 35 kDa, as shown Fig. 4. Anti-sense mouse HRLRRP cDNA (Fig. 4) or reaction mixtures containing no DNA template generated no protein (data not shown).

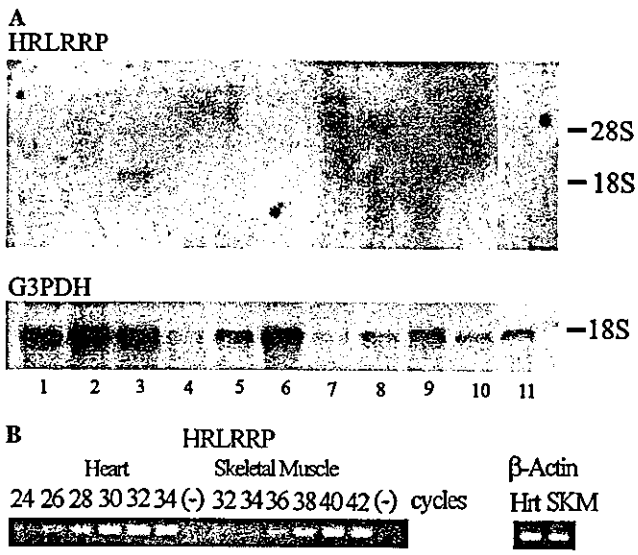


Fig. 2. (A) Northern blot analysis of mouse HRLRRP mRNA in various mouse organs. Detection was made by HRLRRP and G3PDH cDNA probes labeled with biotin. 1, Cerebrum; 2, cerebellum; 3, heart; 4, lung; 5, liver; 6, kidney; 7, spleen; 8, stomach; 9, colon; 10, small intestine; and 11, skeletal muscle. (B) RT-PCR analysis of HRLRRP and β-actin in heart and skeletal muscle. (–) No reverse transcription and 42 cycles of PCR; Hrt, heart; and SKM, skeletal muscle.

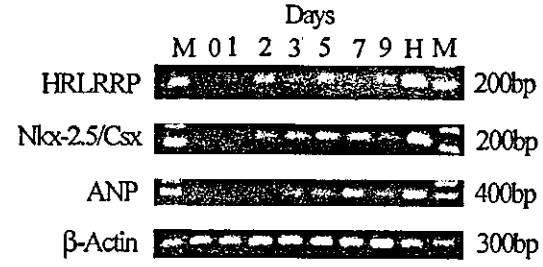


Fig. 3. Gene expression of mouse HRLRRP, Nkx-2.5/Csx, and ANP in the differentiation of DMSO-treated P19CL6 cells to cardiomyocytes. H, adult mouse heart; M, 100-bp ladder marker.

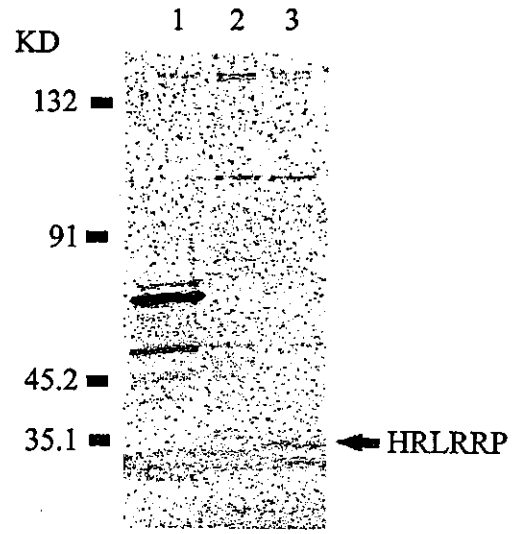


Fig. 4. In vitro transcription/translation of mouse HRLRRP cDNA. Mouse HRLRRP cDNA was in vitro transcribed/translated as described in Materials and methods. 1, Luciferase T7 control DNA; 2, pBK-CMV-anti-HRLRRP; and 3, pcDNA-HRLRRP.

*Mammalian cell expression*

To determine where mouse HRLRRP became localized in cells, we transfected COS7 cells with pQBI-HRLRRP and pFLAG-HRLRRP. Confocal microscopy showed that HRLRRP-GFP was localized in the nucleus and in the mitochondria, which were counterstained with Hoechst 33342 and Mitotracker, respectively (Fig. 5). Anti-FLAG M2 antibody also detected the HRLRRP-FLAG protein in mitochondria but gave only background in the cells transfected with pFLAG-CMV-5b vectors (data not shown). HRLRRP-GFP was detected in the nucleus of some COS7 cells (Fig. 5A) and localized in the mitochondria in most cells (Fig. 5B) 24 and 48 h, respectively, after the transfection. Some COS7 cells transfected with HRLRRP expression vectors became shrunken after 48 h and Mitotracker stained the mitochondria in these shrunken COS7 cells, as shown in Fig. 5B.

*Immunohistochemistry*

Some nuclei of the adult mouse heart were strongly stained by the antibody raised against the synthetic peptide of HRLRRP as shown Fig. 6. No significant immune reactivity was detected when preimmune serum

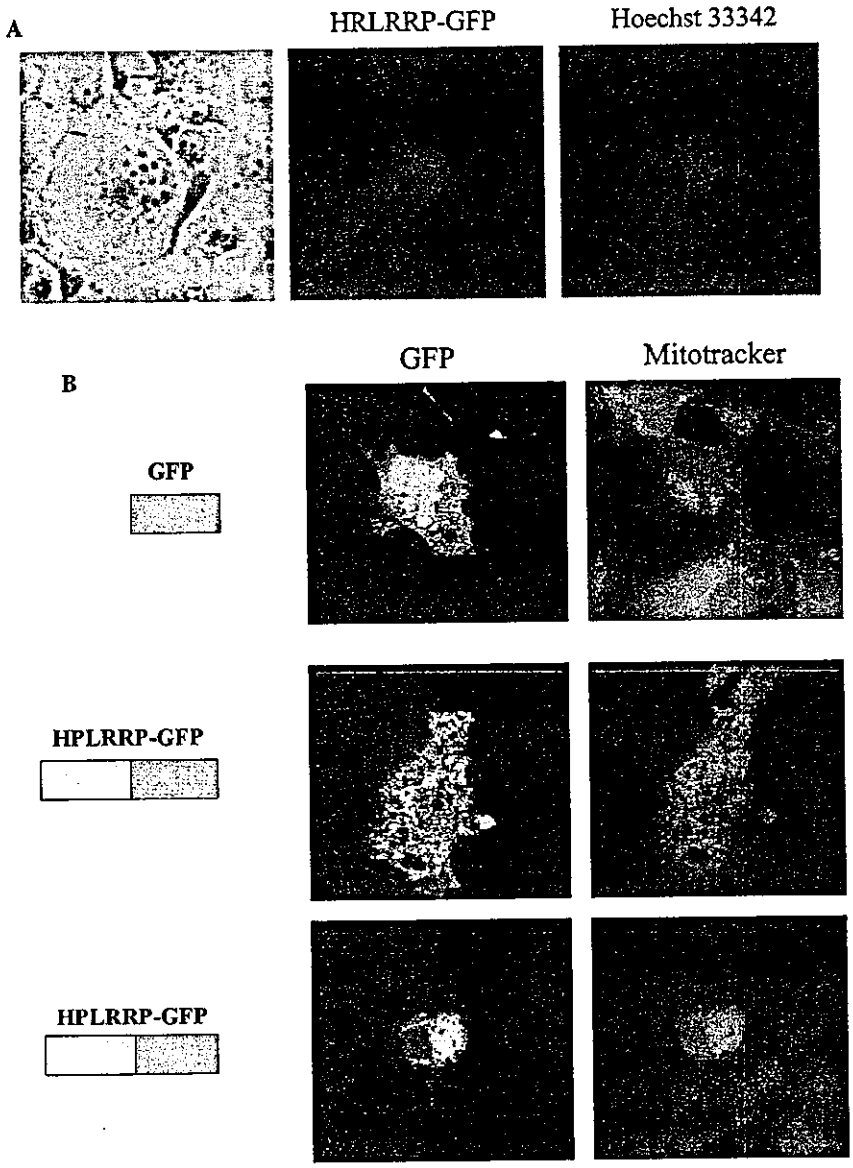


Fig. 5. Expression of mouse HRLRRP-GFP fusion protein in COS7 cells. COS7 cells were transfected with pQBI-HRLRRP for transient expression of HRLRRP-GFP under the control of the cytomegalovirus promoter. Staining with Hoechst 33342 at 24 h (A) and with Mitotracker at 48 h (B) after transfection with pQBI-HRLRRP-GFP and fluorescence detection were conducted. Cells were observed by fluorescence microscopy (A) and by confocal microscopy (B).

was used. Slight immunoreactivities were detected in some nuclei of skeletal muscle and liver (data not shown). Significant immunoreactivity was not observed in the nuclei and mitochondria of P19CL6 and COS7 cells when both the preimmune serum and the anti-HRLRRP antibody were used (data not shown).

## Discussion

We cloned a cDNA encoding mouse heart-restricted leucine-rich repeat protein (HRLRRP) from mouse E13 embryos by the in silico approach. We showed by Northern blotting that the transcripts of *HRLRRP* were detected only in the heart among adult mouse tissues, and by RT-PCR that at the early stage of the differentiation of P19CL6 embryonal carcinoma cells into cardiac muscle. HRLRRP-GFP was localized in nuclei and mitochondria of COS7 cells. Strong nuclear staining was observed with the antibody for the synthetic peptide of HRLRRP in the adult mouse heart.

The cDNA of mouse HRLRRP was 1257 bp in length and the sequence agreed with those of mouse (AF527781 and AK085779) mRNA clones and mouse genomic clone of chromosome 15 (AL589661). The sequence was mapped to mouse chromosome 10 (LocusID 237560). NCBI classified the gene as leucine-rich containing 10 (Lrrc10). The gene showed no intron when the cDNA

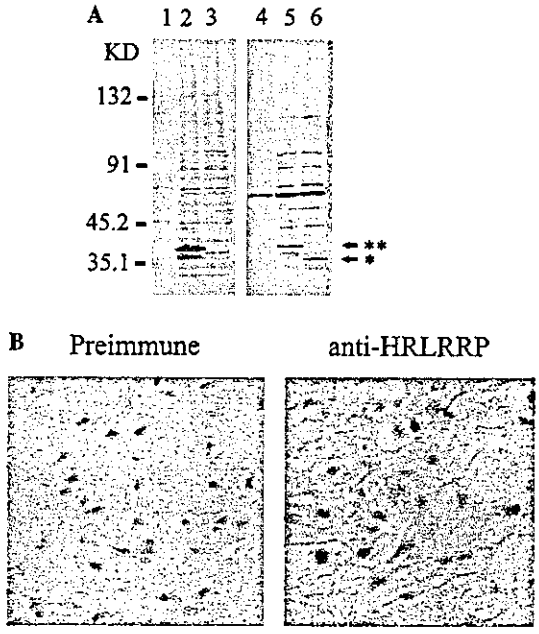


Fig. 6. (A) Western blot analysis of COS7 cells were transfected with pFLAG-HRLRRP (lanes 2 and 5) and pME18S-HRLRRP (lanes 3 and 6) for transient expression of HRLRRP (*) and HRLRRP-FLAG (**). No vector transfection control (lanes 1 and 4). After 48 h, the cells were lysed and used for the analysis. Mouse anti-FLAG M2 and rabbit anti-HRLRRP antibodies were used in lanes 1–3 and 4–6, respectively. (B) Immunostainings of the adult mouse heart were performed with the preimmune serum and anti-HRLRRP antibody.

sequence was compared with the genomic one (NP666354). When mouse genomic DNA was amplified by HRLRRP full-length primers (3882LF and 3882LR), the length of its PCR products was not different from that of the cDNA (data not shown). Transcripts of approximately 1.3 kb were detected only in the heart by Northern blot analysis (Fig. 2A). However, slight expression of HRLRRP mRNA was detected in mouse skeletal muscle by RT-PCR (Fig. 2B). Some of the nuclei of the adult mouse heart were strongly stained by the anti-HRLRRP antibody (Fig. 6B), but those of the skeletal muscle and liver were weakly stained. Therefore, we designated this protein as heart-restricted leucine-rich repeat protein (HRLRRP). Mouse HRLRRP mRNA has a long 3′-untranslated region that may have another potential open reading frame (Fig. 1A). The results of the in vitro transcription/translation study showed that the molecular weight of mouse HRPLRRP was less than 35 kDa (Fig. 3). Therefore, we think that this cDNA really encodes mouse HRPLRRP.

Mouse *HRLRRP* encodes a protein of approximately 31 kDa that contains 7 leucine-rich repeat (LRR) motifs [19], as shown in Table 1 and Fig. 1B. The LRR motif is a protein–protein interaction domain found in many proteins with diverse cellular functions such as hormone–receptor interactions, enzyme inhibition, cell adhesion, and cellular trafficking [20]. Recent studies have implicated LRR proteins in early mammalian development [21], neural development [22], cell polarization [23], regulation of gene expression [24], and apoptosis signaling [25]. HRLRRP showed no significant homology with any domain other than LRR. The LRR proteins often contain multiple distinct domains such as Acan125, which contains LRR and PXXP domains [26]; flightless, which has LRR and gelsolin [27]; and LRDD, which contains LRR and a death domain [28]. HRLRRP may thus bind specific partners in a complex. Because of the absence of catalytic domains, HRLRRP does not have any enzymatic function. HRLRRP may act as an adaptor protein that allows for the formation of a specific complex, which in turn plays a positive role in some aspect of cardiac development or the cardiac function.

Strong nuclear staining was observed with the anti-HRLRRP antibody in the adult mouse heart. Mouse HRLRRP-GFP was localized in nuclei and mitochondria of COS7 cells when it was forced to express. At 24 h after the transfection of COS7 cells with pQBI-HRLRRP, HRLRRP-GFP localized in the nuclei of a few COS7 cells and mitochondria. At 48 h after the transfection, the fusion protein seemed to reside in the mitochondria of most COS7 cells. Because the accumulation of HRLRRP-GFP in the mitochondria was larger than that in the nucleus due to the forced expression of HRLRRP, it seemed that the protein was not located significantly in the nucleus. In the present study, HRLRRP does not exist in mitochondria of the adult mouse heart at the high concentration, but it is not clear whether the protein is localized in mitochondria or not. Then, further histological studies are needed. Other LRR proteins were found in the nucleus, cytoplasm, plasma membrane, and extracellular matrix [29]. A novel leucine-rich pentatricopeptide repeat-motif-containing protein (LRPPRC) appeared in both cytosol and nuclei of cultured cells [30]. Based on their analysis of the binding of proteins to LRPPRC, Liu et al. [30] speculated that the LRPPRC complex may be involved in mitochondrial trafficking and that associations with these binding proteins may be stimulatory or quenching for transcription, growth, and differentiation. Therefore, HRLRRP also may affect gene expression, growth, and differentiation of cardiac myocytes and may be implicated in mitochondrial trafficking by binding to other proteins.

In conclusion, we isolated a mouse HRPLRRP cDNA that encoded a 31-kDa protein. The expression of the gene was restricted to the heart and was induced by DMSO-treatment of P19CL6 EC cells. The protein was localized in nuclei of adult mouse heart and in mitochondria and nuclei of COS7 cells forced to express HRLRRP. Therefore, it may play important roles in cardiac development and function. Further studies are needed for a more thorough understanding of HRLRRP.

## References


[1] A.P. Beltrami, K. Urbanek, J. Kajstura, S.M. Yan, N. Finato, R. Bussani, B. Nadal-Ginard, F. Silvestri, A. Leri, C.A. Beltrami, P. Anversa, Evidence that human cardiac myocytes divide after myocardial infarction, N. Engl. J. Med. 344 (2001) 1750–1757.

[2] D. Orlic, J. Kajstura, S. Chimenti, I. Jakoniuk, S.M. Anderson, B. Li, J. Pickel, R. McKay, B. Nadal-Ginard, D.M. Bodine, A. Leri, P. Anversa, Bone marrow cells regenerate infarcted myocardium, Nature 410 (2001) 701–705.

[3] G. Condorelli, U. Borello, L. De Angelis, M. Latronico, D. Sirabella, M. Coletta, R. Galli, G. Balconi, A. Follenzi, G. Frati, M.G. Cusella De Angelis, L. Gioglio, S. Amuchastegui, L. Adorini, L. Naldini, A. Vescovi, E. Dejana, G. Cossu, Cardiomyocytes induce endothelial cells to trans-differentiate into cardiac muscle: implications for myocardium regeneration, Proc. Natl. Acad. Sci. USA 98 (2001) 10733–10738.

[4] M.E. Pownall, M.K. Gustafsson, C.P. Emerson Jr., Myogenic regulatory factors and the specification of muscle progenitors in vertebrate embryos, Annu. Rev. Cell. Dev. Biol. 18 (2002) 747–783.

[5] D. Srivastava, E.N. Olson, A genetic blueprint for cardiac development, Nature 407 (2001) 221–226.

[6] M.H. Parker, P. Seale, M.A. Rudnicki, Looking back to the embryo: defining transcriptional networks in adult myogenesis, Nat. Rev. Genet. 4 (2003) 497–507.

[7] T.J. Lints, L.M. Parsons, L. Hartley, I. Lyons, R.P. Harvey, Nkx-2.5: a novel murine homeobox gene expressed in early heart progenitor cells and their myogenic descendants, Development 119 (1993) 419–431.

[8] I. Komuro, S. Izumo, Csx: a murine homeobox-containing gene specifically expressed in the developing heart, Proc. Natl. Acad. Sci. USA 90 (1993) 8145–8149.

[9] Y. Saga, N. Hata, S. Kobayashi, T. Magnuson, M.F. Seldin, M.M. Taketo, MesP1: a novel basic helix-loop-helix protein expressed in the nascent mesodermal cells during mouse gastrulation, Development 122 (1996) 2769–2778.

[10] T. Hosoda, K. Monzen, Y. Hiroi, T. Oka, E. Takimoto, Y. Yazaki, R. Nagai, I. Komuro, A novel myocyte-specific gene Midori promotes the differentiation of P19CL6 cells into cardiomyocytes, J. Biol. Chem. 276 (2001) 35978–35989.

[11] C.F. Peng, Y. Wei, J.M. Levsky, T.V. McDonald, G. Childs, R.N. Kitsis, Microarray analysis of global changes in gene expression during cardiac myocyte differentiation, Physiol. Genomics 9 (2002) 145–155.

[12] S.V. Anisimov, K.V. Tarasov, D. Riordon, A.M. Wobus, K.R. Boheler, SAGE identification of differentiation responsive genes in P19 embryonic cells induced to form cardiomyocytes in vitro, Mech. Dev. 117 (2002) 25–74.

[13] D. Wang, P.S. Chang, Z. Wang, L. Sutherland, J.A. Richardson, E. Small, P.A. Krieg, E.N. Olson, Activation of cardiac gene expression by myocardin, a transcriptional cofactor for serum response factor, Cell 105 (2001) 851–862.

[14] Y. Okazaki, M. Furuno, T. Kasukawa, J. Adachi, H. Bono, S. Kondo, I. Nikaido, N. Osato, R. Saito, H. Suzuki, I. Yamanaka, H. Kiyosawa, et al., Analysis of the mouse transcriptome based on functional annotation of 60,770 full-length cDNAs, Nature 420 (2002) 563–573.

[15] A. Habara-Ohkubo, Differentiation of beating cardiac muscle cells from a derivative of P19 embryonal carcinoma cells, Cell Struct. Func. 21 (1996) 101–110.

[16] P. Chomczynski, N. Sacchi, Single-step method of RNA isolation by acid guanidinium thiocyanate–phenol–chloroform extraction, Anal. Biochem. 162 (1987) 156–159.

[17] T. Nakane, Y. Inada, F. Ito, N. Itoh, S. Tazawa, S. Chiba, Cloning and expression of mouse deafness dystonia peptide 1 cDNA, Biochem. Biophys. Res. Commun. 273 (2000) 759–764.

[18] K. Nakai, P. Horton, PSORT: a program for detecting sorting signals in proteins and predicting their subcellular localization, Trends Biochem. Sci. 24 (1999) 34–35.

[19] L. Patthy, Detecting homology of distantly related proteins with consensus sequences, J. Mol. Biol. 198 (1987) 567–577.

[20] S.G. Buchanan, N.J. Gay, Structural and functional diversity in the leucine-rich repeat family of proteins, Prog. Biophys. Mol. Biol. 65 (1996) 1–44.

[21] Z.B. Tong, L.M. Nelson, J. Dean, Mater encodes a maternal protein in mice with a leucine-rich repeat domain homologous to porcine ribonuclease inhibitor, Mamm. Genome 11 (2000) 281–287.

[22] H. Mutai, Y. Toyoshima, W. Sun, N. Hattori, S. Tanaka, K. Shiota, PAL31, a novel nuclear protein, expressed in the developing brain, Biochem. Biophys. Res. Commun. 274 (2000) 427–433.

[23] D. Bilder, N. Perrimon, Localization of apical epithelial determinants by the basolateral PDZ protein Scribble, Nature 403 (2000) 676–680.

[24] M.W. Linhoff, J.A. Harton, D.E. Cressman, B.K. Martin, J.P. Ting, Two distinct domains within CIITA mediate self-association: involvement of the GTP-binding and leucine-rich repeat domains, Mol. Cell. Biol. 21 (2001) 3001–3011.

[25] N. Inohara, T. Koseki, L. del Peso, Y. Hu, C. Yee, S. Chen, R. Carrio, J. Merino, D. Liu, J. Ni, G. Nunez, Nod1, an Apaf-1-like activator of caspase-9 and nuclear factor-κB, J. Biol. Chem. 274 (1999) 14560–14567.

[26] P. Xu, K.I. Mitchelhill, B. Kobe, B.E. Kemp, H.G. Zot, The myosin-I-binding protein Acan125 binds the SH3 domain and belongs to the superfamily of leucine-rich repeat proteins, Proc. Natl. Acad. Sci. USA 94 (1997) 3685–3690.

[27] H.D. Campbell, T. Schimansky, C. Claudianos, N. Ozarac, A.B. Kasprzak, J.N. Ctsell, I.G. Young, H.G. de Couet, G.L. Miklos, The *Drosophila melanogaster* flightless-I gene involved in gastrulation and muscle degeneration encodes gelsolin-like and leucine-rich repeat domains and is conserved in *Caenorhabditis elegans* and humans, Proc. Natl. Acad. Sci. USA 90 (1993) 11386–11390.

[28] J.B. Telliez, K.M. Bean, L.L. Lin, LRDD, a novel leucine rich repeat and death domain containing protein, Biochim. Biophys. Acta 1478 (2000) 280–288.

[29] B. Kobe, J. Deisenhofer, The leucine-rich repeat: a versatile binding motif, Trends Biochem. Sci. 19 (1994) 415–421.

[30] L. Liu, V. Amy, G. Liu, W.L. McKeehan, Novel complex integrating mitochondria and the microtubular cytoskeleton with chromosome remodeling and tumor suppressor RASSF1 deduced by in silico homology analysis, interaction cloning in yeast, and colocalization in cultured cells, In Vitro Cell Dev. Biol. Anim. 38 (2002) 582–594.

Virchows Arch (2004) 444:304–306
DOI 10.1007/s00428-003-0957-1

LETTER TO THE EDITOR

**Akihiko Yoshizawa · Hiroyoshi Ota · Nobuki Sakaguchi · Shinichiro Kanai · Jun Nakayama · Kenji Matsuzawa · Shigetoshi Tsuzuki · Reiko Takada · Fujie Miyazawa · Hiroko Kasahara · Tsutomu Katsuyama**

# Malignant granular cell tumor of the esophagus

Received: 4 February 2003 / Accepted: 28 November 2003 / Published online: 24 January 2004


Sir, We have recently encountered an interesting case of a malignant granular cell tumor of the esophagus. The patient was a 71-year-old man who died of malignant granular cell tumor of the esophagus with pleural effusion and multiple liver metastases.

The patient presented complaining of dysphagia for the past 10 months. A barium swallow showed a filling defect in the lower part of esophagus. Esophagogastroendoscopy showed a submucosal tumor with central ulceration located 35 cm distal from the incisor teeth. The computed tomography scan (CT) of his chest revealed a solid tumor mass measuring 6×4 cm in diameter with obstruction in the mid-esophagus. Biopsies of this area demonstrated a granular cell tumor. The patient subsequently underwent an esophagogastrectomy.

The resected esophagus revealed a submucosal tumor in the mid-esophagus. It was a poorly defined mass, measuring 10×5 cm in length, with circumferential involvement. At the cut surface, the tumor was white, firm and involved beyond the proper muscle layer into the adventitia.

Microscopically, tumor cells mainly grew in the submucosa and infiltrated beyond the proper muscle layer into the adventitia. The surgical margin was free of tumor cells. Pseudoepitheliomatous hyperplasia of the squamous epithelium overlying esophageal tumor was present.

The tumor cells were arranged in small clusters divided by thin fibrous connective tissue septa (Fig. 1). The tumor cells showed oval, polygonal or spindle-shaped cytoplasm with abundant eosinophilic cytoplasmic granules (Fig. 1). Occasional mitotic figures were seen (mitotic index: 0.3%) (Fig. 1). In some areas, the tumor cells showed nuclear pleomorphism with prominent nuclear atypia. Small necrotic foci were present. Oval-shaped tumor cells with small blunt nuclei were noted to proliferate in the lamina propria, just beneath the esophageal epithelium. Lymph-node metastasis was not observed. Immunohistochemically, most tumor cells were positive for S-100 protein (Dako, CA, USA), keratan sulfate (Seikagaku Kogyo, Japan), neuron specific enolase (Dako), CD68 (Dako), and vimentin (Dako), and about one-third of tumor cells were positive for CD57 (Beckton Dickinson, CA, USA). Collagen type IV (Dako) was demonstrated around nests of tumor cells. The tumor cells showed no reactivity for carcinoembryonic antigen (Dako), myelin basic protein (Dako), CD34 (Dako), c-kit (Dako), chromogranin A (Dako), synaptophysin (Dako) and p53 (Dako). The tumor cells showed a higher Ki67 value (8.3%±2.1) than five cases of benign granular cell tumors used as controls (3.3%±2.9). In addition, the tumor cells with small blunt nuclei in the lamina propria, just beneath the esophageal epithelium, showed lower proliferative activity than the tumor cells showing pleo-

A. Yoshizawa · S. Kanai
Department of Laboratory Medicine,
Shinshu University Hospital,
Matsumoto, Japan

H. Ota (✉)
Department of Biomedical Laboratory Sciences,
School of Health Sciences and Department of Laboratory Medicine,
Shinshu University School of Medicine,
3-1-1 Asahi, Matsumoto, 390-8621 Nagano, Japan
e-mail: hohta@gipac.shinshu-u.ac.jp
Tel.: +81-26-3372389
Fax: +81-26-3372389

N. Sakaguchi
First Department of Internal Medicine,
Shinshu University School of Medicine,
Matsumoto, Japan

J. Nakayama
Department of Pathology and Department of Laboratory Medicine,
Shinshu University School of Medicine,
Matsumoto, Japan

K. Matsuzawa · S. Tsuzuki · R. Takada · F. Miyazawa · H. Kasahara
Maruko Chuo General Hospital,
Maruko, Japan

T. Katsuyama
Department of Laboratory Medicine,
Shinshu University School of Medicine,
Matsumoto, Japan